Università degli Studi di Milano - Bicocca
Facoltà di Scienze Matematiche, Fisiche e Naturali
Corso di Dottorato di Ricerca in Scienza dei Materiali,
curriculum industriale
XXII ciclo

Metamaterials based on photonic quasicrystals: from superlensing to new photonic devices

---

A.A. 2008/2009

Ph.D. dissertation
Luca Maini

Supervisor
Prof. Giorgio Benedek

Contents

Acknowledgements

I would like to thank my supervisor Prof. Giorgio Benedek for the guide and support during my Ph.D. work.

The work presented in this thesis was started in collaboration with Dr. Vincenzo Boffa, Dr. Giuseppe Grassano and Dr. Fabrizio Ricci at Pirelli Labs who introduced me to the subject and gave me the possibility to collaborate with the experimental group of Prof. Antonello Andreone and Dr. Emiliano Di Gennaro at the Università degli Studi di Napoli Federico II.

I would like to thank Dr. Javier Aizpurua for the support and discussions during my stay at the Donostia International Physics Center (DIPC) in San Sebastián.

I wish to thank also my ex-supervisors and friends Dr. Mario Italo Trioni and Dr. Francesco Montalenti for the scientific and non-scientific discussions, suggestions and advices throughout the years.

This work wouldn't have been possible with the neverending support of my family.

Chapter 1

Introduction

Metamaterials are defined as a class of ordered composites that exhibit exceptional properties that arise from qualitatevely new response functions, that are not observed in the constituent materials and result from the inclusion of artificially fabricated, extrinsic, low dimensional inhomogeneities.

This means that if properly engineered, metamaterials can exhibit tailored values of response functions such as the dielectric function ε or the magnetic permeability μ. Tuning the optical proprerties in this way, metamaterials can be used to control electromagnetic waves and structures that can even cloak an object from incident radiations can be fabricated.[1]

Modifying the values of ε and μ has as a direct consequence the modification of the value of the index of refraction n of the metamaterial, which in turn is another response function that can be tuned in this particular class of materials.

It has to be noted though that the index of refraction n can be tuned without varying the values of ε and μ throughout the entire structure, but also simply using two (or more) constituent materials with different response function, ordered in a lattice. This is precisely what happens in *photonic crystals*, ordered structures made of dielectric or metals, that can be realized in one, two or three dimensions.[2]

1.1 Photonic Crystals

In order to define what is a photonic crystal, we rely on an analogy with electronic materials, where a crystal is a periodic arrangement of atoms or molecules. The pattern with which the atoms or molecules are repeated in space is the crystal lattice. The crystal presents a periodic potential to an electron propagating through it, and both the constituents of the crystal and the geometry of the lattice dictate the conduction properties of the crystal. Electrons propagate as waves, and waves that meet certain criteria can travel through a periodic potential without scattering, unless the crystal is not perfect: in presence of defects and impurities electron waves will be scattered.

The lattice can also prohibit the propagation of certain waves. There may be gaps in the energy band structure of the crystal, meaning that electrons are forbidden to propagate with certain energies in certain directions. If the lattice potential is strong enough, the gap can extend to cover all possible propagation directions, resulting in a complete band gap. For example, a semiconductor has a complete band gap between the valence and conduction energy bands.

The optical analogue is the photonic crystal, in which the atoms or molecules are replaced by macroscopic media with differing dielectric constants, and the periodic potential is replaced by a periodic dielectric function. Following the analogy with electron waves propagating in a crystal, light waves traveling in periodic structures will be described in terms of photonic bands with the possibility of the existence of frequency gaps where the propagation of electromagnetic waves is forbidden.

If, for some frequency range, a photonic crystal prohibits the propagation of electromagnetic waves of any polarization traveling in any direction from any source, we say that the crystal has a complete photonic band gap. A small amount of disorder in an otherwise periodic medium will not destroy a band gap, and even a highly disordered medium can prevent propagation in a useful way through the mechanism of Anderson

localization.[3,4]

More or less ordered photonic crystals have been recognized in recent years to be largely diffused in nature, where they provide an immense variety of structural colorations to coleopters, butterfly wings, etc.,[5–7] and a source of inspiration for novel bio-mimetic nanotechnologies for color engineering and photonic devices.[8] Among the interesting non-periodic classes of materials that can have complete phononic band gaps there are the quasi-crystalline structures.

1.2 Quasicrystals

Discovered not a long time ago,[9,10] quasicrystals are quasiperiodic structures, in the sense that they are non-crystalline materials with perfect long-range order, but without any kind of translational periodicity.

Even in the absence of lattice periodicity, quasicrystals exhibit sharp discrete peaks in the diffraction diagram, indicating the presence of rotational symmetry and long-range order. Of particular interest is the possible inclusion of rotational symmetries such as 5, 8, 10 or 12-fold that are incompatible with periodicity.

Quasicrystals exists in one, two or three dimensions but their description in terms of reciprocal lattice vectors and diffraction patterns requires moving to a higher dimensional space where they can be treated as a periodic structure. Another way to tackle the problem of describing quasiperiodic systems rely on the concept of periodic approximants, where a portion of the quasicrystal is considered appropriate to represent the whole infinite structure.[11]

1.3 Photonic Quasicrystals

Photonic quasicrystal are simply an extension of the concept of photonic crystal: instead of being based on a periodic lattice, they rely on a *quasi*periodic pattern of the dielectric media. The peculiar properties of

the quasiperiodic order in photonic structures, such as higher rotational symmetry and intrinsic presence of defects, recently attracted some interest.[12–18]

In this thesis we focus our study on metamaterials based on 12-fold photonic quasicrystal from the computational point of view trying to have an insight of their optical properties and response, with the aim of providing informations and ideas useful to the realization of new photonic devices.

Chapter 2

Negative Refraction

Recently, negative refraction has attracted a great deal of attention, largely due to the realization that this phenomenon could lead to the development of a perfect lens, also called *superlens*.[19] A perfect lens is supposed to be able to focus all Fourier components, i.e. both the propagating and evanescent modes, of a two dimensional image without missing any details or losing any energy. Althought such a lens has yet to be shown possible either physically and pratically, the interest has generated considerable research in electromagnetism and various interdisciplinary areas in terms of fundamental physics and material science.[20,21] Negative refraction, as a physical phenomenon, may have much broader implications than making a perfect lens: different approaches used to achieve negative refaction may involve very different physics and may find unique applications in different technology areas.

The group velocity of a wave, $\mathbf{v}_g(\omega, \mathbf{k}) = d\omega/d\mathbf{k}$, is often used to describe the direction and the speed of its energy propagation. For an electromagnetic wave, strictly speaking, the energy propagation is determined by the Poynting vector $\mathbf{S}$. For a quasimonochromatic wave packet in a medium without external sources and with negligible distorsion and absorption, the direction of S does concide with that of $\mathbf{v}_g$.[22] The angle between $\mathbf{v}_g$ and wave vector $\mathbf{k}$ distinguish two types of media: when the angle is acute or $\mathbf{k} \cdot \mathbf{v}_g > 0$, it is said to be a right-handed medium (RHM); when the angle is obtuse or $\mathbf{k} \cdot \mathbf{v}_g < 0$, it is said to be a left-handed medium (LHM).[23]

Unusual physical phenomena are expected to emerge either in an individual LHM, as a reversal of both the group velocity and Doppler

shift, or in combination with an RHM, where the interface of the two media gives rise to negative refraction.[23] This latter effect is the one that attracted most attention lately ad relies on the property $\mathbf{k} \cdot \mathbf{v}_g < 0$ in the LHM.

2.1 Negative Refraction with Double Negativity

The simplest way to produce LH behaviour is to use a medium with both $\varepsilon < 0$ and $\mu < 0$, since double negativity requires energy to flow away from the interface and into the medium.[23] Furthermore, it was demonstrated[23,24] that a LH medium has a negative refractive index $\sqrt{n} = \sqrt{\varepsilon} \cdot \sqrt{\mu}$, leading to negative refraction at the interface with an RHM.

Real material however have $\varepsilon < 0$ only near the resonant frequency of a polariton; without damping the spectral region of $\varepsilon < 0$ is totally reflective for materials with $\mu > 0$. $\mu < 0$ is also known to exist near magnetic resonances, but is not known to occur in the same material and the same frequency region where $\varepsilon < 0$ is found.

In recent years, metamaterials have been developed to extend material response and thus allow effective ε and μ to be negative in an overlapped frequency region.[21] The hybridization of the metamaterials with $\varepsilon_{\text{eff}} < 0$ and $\mu_{\text{eff}} < 0$ has made it possible to realize double negativity or $n_{\text{eff}} < 0$ in a small frequency window, and to demonstrate negative refraction successfully.[25,26]

In this type of artificial materials, since they operate near the magnetic resonance, high loss is expected; furthermore, the wavelength is much larger than the lattice constant, and for this reason the push to higher frequencies may be limited to the THz range.[27–29] The physics behind this limit is that any material will have $\mu \to 1$ since the electrons will not keep pace with the frequency of visible light.[30]

2.2 Negative Refraction using Photonic Crystals

Another class of material that can show negative refraction are photonic crystals, often described as artificial periodic structures,[2] made of dielectric or metal, designed to control photons simliar to the way a solid-state crystal controls electrons. It has been proposed that negative refraction can be achieved in photonic crystals with lattice constant comparable to the wavelength.[31,32]

Locally both $\varepsilon, \mu > 0$ everywhere in photonic crystals; the physical principles that allow negative reference arise from the dispersion characteristics of wave propagation in a periodic medium, and are very different from that of the double negative materials previously described. To have the desired dispersion characteristic for negative refraction, large dielectric constant contrast could be required, but this doesn't impose any fundamental limit on pushing negative refraction in photonic crystals towards visible frequency range, infrared spectral range being already reported.[33]

Photonic crystals exhibit a diffractive behaviour where electromagnetic waves behave following dispersion relations $\omega_n(\mathbf{k})$, where n is the band index, and $\mathbf{k}$ is the wave vector in the first Brillouin zone, as will be described more in detail in section 4.4.

For a two or three dimensional photonic crystal, the direction of the energy flux, averaged over the unit cell, is determined by the group velocity $d\omega_n(\mathbf{k})/d\mathbf{k}$. If the dispersion is isotropic, the condition $\mathbf{q} \cdot d\omega_n(\mathbf{q})/d\mathbf{q} < 0$ where $\mathbf{q}$ is the wave vector measured from a local extremum, must be satisfied to have LH behaviour. This condition allows the occurrence of negative refraction at the interface of air and photonic crystal as well as the imaging effect with a flat photonic slab.[31,32,34,35]

2.3 Superlensing

Pendry pointed out that the distinguishing feature of double negativity matierals, compared to other schemes that can achieve negative refraction, was the potential for realizing a perfect lens beyond negative refraction.[19]

However, such a perfect lens, in addition to negative refraction, should possess three crucial features: zero dissipation, amplification of evanescent waves and matching of the dielectric parameters at the interface between the lens and air. Exactly zero dissipation it unfortunately physically impossible for any real material, and even a very weak absorption will certainly make the lens imperfect.

Mathematically, double negativity materials are the only ones that provide a correct amount of amplification for each evanescent wave.[19] On the other hand, this type of materials become problematic at high frequencies because of the ambiguity in defining nonunity μ at high frequencies.[30,36] Photonic crystals may also amplify the evanescent components when the effective refractive index $n_{\text{eff}} < 0$ keeping in mind that some complications are present, tipically the amplification magnitude might not be exactly correct or the resolution is limited by the periodicity of the photonic crystal.[37]

One important requirement of negative refraction for making a perfect lens is matching the dielectric parameters of the two media to eliminate reflection and aberration: in the case of double negativity material, this condition becomes $n_1 = -n_2$. Another limitation comes from frequency dispersion, which prohibits the matching condition of the dielectric parameters to remain valid in a broad frequency range; in the case of photonic crystals also the effective index is frequency dependent. Therefore, even for the ideal case of vanishing damping, the matching condition can be found at best for discrete frequencies.

However, even with the practical limitations on these three aspects - damping, incorrect magnitude of amplification and dielectric mismatch

- one can still be hopeful of achieving a finite improvement in focusing light beyond the usual diffraction limit,[38] in addition of the benefits of having a flat lens. The primary advantage of the *superlens* seems to be the ability to achieve subwavelength focusing with both the source and image at far field. Thus far, using negative refraction, there have been only a few experimental demonstration of non-near-field imaging with improved resolution.[14,39] On a side note, plasmonic systems such as ultra thin metal films have also been used to achieve subwavelength imaging in near field,[40,41] although not necessarily related to negative refraction.

The focusing power of a lens usually refers to the ability to provide an image smaller than the object. What the hypothetical flat lens can do is exactly reproduce the source at the image site or, in other words, spatially translate the source by a distance $2d$ where d is the thickness of the slab. Thus, mathematically, a δ-function source will give rise to a δ-function image, without being subjected to the diffraction limit of a regular lens $\lambda/2$.[42] Such a *superlens* in principle can resolve two objects with any nonzero separation, overcoming the Rayleigh criterion of 0.61λ for the resolving power of a regular lens.[42]

However, what this *superlens* cannot do is focus an object greater than λ to an image smaller than λ. Therefore it might not be appropriate to call such optical device with no magnification a *lens*. In practice, a *superlens* could be used to map or translate a light source, while retaining its size that could be already below the diffraction limit.

2.4 Negative Refraction and Imaging with Quasicrystals

Relating to imaging and focusing there are two relevant aspects: position (in near-field or non-near-field region) and resolution (full width at half maximum of the focus spot). The position of the image depends on the effective refractive index n_{eff} of the sample and the homogeneity of

the materials. In the case of $n_{\text{eff}} = -1$ and single-mode transmission, the imaging behavior depends on the slab thickness and the object distance, explicitly following the well known wave-beam negative refraction law.[43–45]

However, due to the anisotropy of dispersion in some 2D photonic crystals, the refraction angles are not linearly proportional to the incident angles when a plane wave is incindent from vacuum to the photonic crystal. This is the reason why only the near-field images were observed in some works.[32,34,35,46–50] The position of the image does not depend on whether or not the evanescent waves are amplified, and the focus and the image can still be observed if only the propagating waves are considered. In such a case, the image resolution cannot overcome the diffraction limit. The superlensing effect comes from the evanescent waves: the excitation of surface mode (or the appearance of resonant transmission) can improve the image resolution.[32,48]

It becomes evident that the anisotropy of the dispersion is dipendent on the symmetry of the photonic crystal lattice. In order to obtain homogeneous dispersion and realize the non-near-field focus, we should use the structures with high symmetry to construct a flat lens. However, the highest level of symmetry that can be found in a periodic lattice is six. On the other hand, the geometric symmetry in photonic quasicrystals can reach 12 (or even higher symmetries). It has been noted that the presence of a photonic band gap, one of the most peculiar features of photonic crystals, shows up in photonic quasicrystals too.[12,51,52] For these reasons it seems interesting to investigate photonic quasicrystals to see if they exhibit negative refraction and if this property is less sensitive to the angle of incidence of the electromagnetic wave.

The study of photonic quasicrystals though implies some complications from both the theoretical and the computational point of view, compared to the study of standard periodic photonic crystal. As seen in chapter 1.2, quasicrystals are not periodic, don't have any translational symmetry and thus all the Bloch derived concepts and theory that will

be examined in detail in chapter 4 should be used with care. Calculation based on rational approximants,[53] on extended zone schemes in the reciprocal space[54,55] or on constituent parts of the quasicrystal[13] have been used to investigate properties of photonic quasicrystals, showing band gaps at lower frequencies (in comparison to photonic crystals), gaps at multiple operational frequencies, higher isotropy and ultimately negative refraction and subwavelength focusing effects.[14,56]

Chapter 3

Electromagnetism in mixed media

In order to study the propagation of light in a photonic crystal, we begin with the Maxwell equations. We restrict ourselves to the case of a mixed dielectric medium and we cast the Maxwell equations as a linear Hermitian eigenvalue problem. This brings the electromagnetic problem into a close analogy with the Schrödinger equation, and allows us to take advantage of some well-established results from quantum mechanics. One way in which the electromagnetic case differs from the quantum-mechanical case is that photonic crystals do not generally have a fundamental scale, in either the spatial coordinate or in the potential strength (the dielectric constant). This makes photonic crystals scalable in a way that traditional crystals are not, as we will show in section 4.6.

3.1 The macroscopic Maxwell equations

All of macroscopic electromagnetism, including the propagation of light in a photonic crystal, is governed by the four macroscopic Maxwell equations. In SI units, they are

$$\begin{aligned} \nabla \cdot \mathbf{B} = \mathbf{0} \quad & \nabla \times \mathbf{E} + \frac{\partial \mathbf{B}}{\partial \mathbf{t}} = 0 \\ \nabla \cdot \mathbf{H} = \rho \quad & \nabla \times \mathbf{H} - \frac{\partial \mathbf{D}}{\partial \mathbf{t}} = \mathbf{J} \end{aligned} \tag{3.1}$$

where (respectively) $\mathbf{E}$ and $\mathbf{H}$ are the macroscopic electric and magnetic fields, $\mathbf{D}$ and $\mathbf{B}$ are the displacement and magnetic induction fields, and ρ and $\mathbf{J}$ are the free charge and current densities.

We will restrict ourselves to propagation within a mixed dielectric medium, a composite of regions of homogeneous dielectric material as a function of the (cartesian) position vector $\mathbf{r}$, in which the structure does not vary with time, and there are no free charges or currents. With this type of medium in mind, in which light propagates but there are no sources of light, we can set $\rho = 0$ and $\mathbf{J} = \mathbf{0}$.

Next we relate $\mathbf{D}$ to $\mathbf{E}$ and $\mathbf{B}$ to $\mathbf{H}$ with the constitutive relations appropriate for our problem. Quite generally, the components D_i of the displacement field $\mathbf{D}$ are related to the components E_i of the electric field $\mathbf{E}$ via a power series,

$$D_i/\varepsilon_0 = \sum_j \varepsilon_{ij} E_j + \sum_{j,k} \chi_{ijk} E_j E_k + O(E^3), \tag{3.2}$$

where $\varepsilon_0 \approx 8.854 \times 10^{-12}$ Farad/m is the vacuum permittivity. However, for many dielectric materials, it is reasonable to use the following approximations. First, we assume the field strengths are small enough so that we are in the linear regime, so that χ_{ijk} (and all higher-order terms) can be neglected. Second, we assume the material is macroscopic and isotropic, so that $\mathbf{E}(\mathbf{r}, \omega)$ and $\mathbf{D}(\mathbf{r}, \omega)$ are related by ε_0 multipled by a scalar dielectric function $\varepsilon(\mathbf{r}, \omega)$, also called the relative permittivity. Third, we ignore any explicit frequency dependence (material dispersion) of the dielectric constant. Instead, we simply choose the value of the dielectric constant appropriate to the frequency range of the physical system we are considering. Fourth, we focus primarily on transparent materials, which means we can treat $\varepsilon(\mathbf{r})$ as purely real and positive.

Assuming these four approximations to be valid, we have $\mathbf{D}(\mathbf{r}) = \varepsilon_\mathbf{0}\varepsilon(\mathbf{r})\mathbf{E}(\mathbf{r})$. A similar equation relates $\mathbf{B}(\mathbf{r}) = \mu_\mathbf{0}\mu(\mathbf{r})\mathbf{H}(\mathbf{r})$ (where $\mu_0 = 4\pi \times 10^7$ Henry/m is the vacuum permeability), but for most dielectric materials of interest the relative magnetic permeability $\mu(r)$ is very close to unity and we may set $\mathbf{B} = \mu_\mathbf{0}\mathbf{H}$ for simplicity. In that case, ε is the square of the refractive index n that may be familiar from Snell's law and other formulas of classical optics (in general, $n = \sqrt{\varepsilon\mu}$).

With all of these assumptions in place, the Maxwell equations become

$$\begin{aligned} \nabla \cdot \mathbf{H}(\mathbf{r},t) = 0 \quad & \nabla \times \mathbf{E}(\mathbf{r},t) + \mu_0 \frac{\partial \mathbf{H}(\mathbf{r},t)}{\partial t} = 0 \\ \nabla \cdot [\varepsilon(\mathbf{r})\mathbf{E}(\mathbf{r},t)] = 0 \quad & \nabla \times \mathbf{H}(\mathbf{r},t) - \varepsilon_0 \varepsilon(\mathbf{r}) \frac{\partial \mathbf{E}(\mathbf{r},t)}{\partial t} = 0. \end{aligned} \tag{3.3}$$

In general, both $\mathbf{E}$ and $\mathbf{H}$ are complicated functions of both time and space. Because the Maxwell equations are linear, however, we can separate the time dependence from the spatial dependence by expanding the fields into a set of harmonic modes. In this and the following sections we will examine the restrictions that the Maxwell equations impose on a field pattern that varies sinusoidally (harmonically) with time. This is no great limitation, since we know by Fourier analysis that we can build any solution with an appropriate combination of these harmonic modes. Often we will refer to them simply as *modes* or *states* of the system.

For mathematical convenience, we employ the standard trick of using a complex-valued field and remembering to take the real part to obtain the physical fields. This allows us to write a harmonic mode as a spatial pattern (or *mode profile*) times a complex exponential:

$$\begin{aligned} \mathbf{H}(\mathbf{r},t) &= \mathbf{H}(\mathbf{r})e^{-iwt} \\ \mathbf{E}(\mathbf{r},t) &= \mathbf{E}(\mathbf{r})e^{-iwt}. \end{aligned} \tag{3.4}$$

To find the equations governing the mode profiles for a given frequency, we insert the above equations into 3.3. The two divergence equations give the conditions

$$\nabla \cdot \mathbf{H}(\mathbf{r}) = 0, \qquad \nabla \cdot [\varepsilon(\mathbf{r})\mathbf{E}(\mathbf{r})] = 0, \tag{3.5}$$

which have a simple physical interpretation: there are no point sources or sinks of displacement and magnetic fields in the medium. Equivalently, the field configurations are built up of electromagnetic waves that are transverse. That is, if we have a plane wave $\mathbf{H}(\mathbf{r}) = \mathbf{a}\exp(ik\cdot\mathbf{r})$, for some wave vector $\mathbf{k}$, equation 3.5 requires that $\mathbf{a}\cdot\mathbf{k} = 0$. We can now

focus our attention only on the other two of the Maxwell equations as long as we are always careful to enforce this transversality requirement.

The two curl equations relate $\mathbf{E}(\mathbf{r})$ to $\mathbf{H}(\mathbf{r})$:

$$\begin{aligned} \nabla \times \mathbf{E}(\mathbf{r}) - i\omega\mu_0 \mathbf{H}(\mathbf{r}) &= 0 \\ \nabla \times \mathbf{H}(\mathbf{r}) - i\omega\varepsilon_0 \varepsilon(\mathbf{r}) \mathbf{E}(\mathbf{r}) &= 0. \end{aligned} \tag{3.6}$$

We can decouple these equations in the following way. Divide the bottom equation of 3.6 by $\varepsilon(\mathbf{r})$, and then take the curl. Then use the first equation to eliminate $\mathbf{E}(\mathbf{r})$. Morever, the constants ε_0 and μ_0 can be combined to yield the vacuum speed of light, $c = 1/\varepsilon_0\mu_0$. The result is an equation entirely in $\mathbf{H}(\mathbf{r})$:

$$\nabla \times \left(\frac{1}{\varepsilon(\mathbf{r})} \nabla \times \mathbf{H}(\mathbf{r}) \right) = \left(\frac{w}{c} \right)^2 \mathbf{H}(\mathbf{r}). \tag{3.7}$$

This is the master equation. Together with the divergence equation 3.5, it tells us everything we need to know about $\mathbf{H}(\mathbf{r})$. Our strategy will be as follows: for a given structure $\varepsilon(\mathbf{r})$, solve the master equation to find the modes $\mathbf{H}(\mathbf{r})$ and the corresponding frequencies, subject to the transversality requirement. Then use the second equation of 3.6 to recover $\mathbf{E}(\mathbf{r})$:

$$\mathbf{E}(\mathbf{r}) = \frac{1}{\omega\varepsilon_0\varepsilon(\mathbf{r})} \nabla \times \mathbf{H}(\mathbf{r}) \tag{3.8}$$

Using this procedure guarantees that $\mathbf{E}$ satisfies the transversality requirement $\nabla \cdot \varepsilon\mathbf{E} = 0$, because the divergence of a curl is always zero. Thus, we need only impose one transversality constraint, rather than two. The reason why we chose to formulate the problem in terms of $\mathbf{H}(\mathbf{r})$ and not $\mathbf{E}(\mathbf{r})$ is merely one of mathematical convenience. We note that we can also find $\mathbf{H}$ from $\mathbf{E}$ via the first equation of 3.6:

$$\mathbf{H}(\mathbf{r}) = -\frac{i}{\omega\mu_0} \nabla \times \mathbf{E}(\mathbf{r}) \tag{3.9}$$

3.2 Electromagnetism as an Eigenvalue Problem

As discussed in the previous section, the heart of the Maxwell equations for a harmonic mode in a mixed dielectric medium is a differential equation for $\mathbf{H}(\mathbf{r})$, given by equation 3.7. The content of the equation is this: perform a series of operations on a function $\mathbf{H}(\mathbf{r})$, and if $\mathbf{H}(\mathbf{r})$ is really an allowable electromagnetic mode, the result will be a constant times the original function $\mathbf{H}(\mathbf{r})$. This situation arises often in mathematical physics, and is called an eigenvalue problem. If the result of an operation on a function is just the function itself, multiplied by some constant, then the function is called an eigenfunction or eigenvector of that operator, and the multiplicative constant is called the eigenvalue.

In this case, we identify the left side of the master equation as an operator $\hat{\Theta}$ acting on $\mathbf{H}(\mathbf{r})$ to make it look more like a traditional eigenvalue problem:

$$\hat{\Theta}\mathbf{H}(\mathbf{r}) = \frac{\omega^2}{c^2}\mathbf{H}(\mathbf{r}) \tag{3.10}$$

We have identified $\hat{\Theta}$ as the differential operator that takes the curl, then divides by $\varepsilon(\mathbf{r})$, and then takes the curl again:

$$\hat{\Theta}\mathbf{H}(\mathbf{r}) \triangleq \nabla \times \langle \frac{1}{\varepsilon(\mathbf{r})} \nabla \mathbf{H}(\mathbf{r}) \rangle \tag{3.11}$$

The eigenvectors $\mathbf{H}(\mathbf{r})$ are the spatial patterns of the harmonic modes, and the eigenvalues $\frac{\omega^2}{c^2}$ are proportional to the squared frequencies of those modes. An important thing to notice is that the operator $\hat{\Theta}$ is a linear operator. That is, any linear combination of solutions is itself a solution; if $\mathbf{H_1}(\mathbf{r})$ and $\mathbf{H_2}(\mathbf{r})$ are both solutions of 3.10 with the same frequency ω, then so is $\alpha\mathbf{H_1}(\mathbf{r}) + \beta\mathbf{H_2}(\mathbf{r})$, where α and β are constants. For example, given a certain mode profile, we can construct another legitimate mode profile with the same frequency by simply doubling the field strength everywhere ($\alpha = 2, \beta = 0$). For this reason we consider

two field patterns that differ only by an overall multiplier to be the same mode.

Our operator notation is reminiscent of quantum mechanics, in which we obtain an eigenvalue equation by operating on the wave function with the Hamiltonian. A reader familiar with quantum mechanics might recall some key properties of the eigenfunctions of the Hamiltonian: they have real eigenvalues, they are orthogonal, they can be obtained by a variational principle, and they may be catalogued by their symmetry properties.

All of these same useful properties hold for our formulation of electromagnetism. In both cases, the properties rely on the fact that the main operator is a special type of linear operator known as a Hermitian operator. In the coming sections we will develop these properties one by one. We conclude this section by showing what it means for an operator to be Hermitian. First, in analogy with the inner product of two wave functions, we define the inner product of two vector fields $\mathbf{F}(\mathbf{r})$ and $\mathbf{G}(\mathbf{r})$ as

$$(\mathbf{F}, \mathbf{G}) \triangleq \int d^3\mathbf{r}\mathbf{F}^*(\mathbf{r}) \cdot \mathbf{G}(\mathbf{r}) \tag{3.12}$$

where * denotes complex conjugation. Note that a simple consequence of this definition is that $(\mathbf{F}, \mathbf{G}) = (\mathbf{G}, \mathbf{F})*$ for any $\mathbf{F}$ and $\mathbf{G}$. Also note that $(\mathbf{F}, \mathbf{F})$ is always real and nonnegative, even if $\mathbf{F}$ itself is complex. In fact, if $\mathbf{F}(\mathbf{r})$ is a harmonic mode of our electromagnetic system, we can always set $(\mathbf{F}, \mathbf{F}) = \mathbf{1}$ by using our freedom to scale any mode by an overall multiplier. Given $\mathbf{F}(\mathbf{r})$ with $(\mathbf{F}, \mathbf{F}) \neq \mathbf{1}$, we can create

$$\mathbf{F}(\mathbf{r}) = \frac{\mathbf{F}'(\mathbf{r})}{\sqrt{(\mathbf{F}'(\mathbf{r}), \mathbf{F}'(\mathbf{r}))}} \tag{3.13}$$

From our previous discussion, $\mathbf{F}(\mathbf{r})$ is really the same mode as $\mathbf{F}'(\mathbf{r})$, since it differs only by an overall multiplier, but now we have $(\mathbf{F}, \mathbf{F}) = \mathbf{1}$. We say that $\mathbf{F}(\mathbf{r})$ has been normalized. Normalized modes are very useful in formal arguments. If, however, one is interested in the physical

energy of the field and not just its spatial profile, the overall multiplier is important.

Next, we say that an operator Ξ is Hermitian if $(\mathbf{F}, \Xi\mathbf{G}) = (\Xi\mathbf{F}, \mathbf{G})$ for any vector fields $\mathbf{F}(\mathbf{r})$ and $\mathbf{G}(\mathbf{r})$. That is, it does not matter which function is operated upon before taking the inner product. Clearly, not all operators are Hermitian. To show that $\hat{\Theta}$ is Hermitian, we perform an integration by parts[a] twice:

$$\begin{aligned}(\mathbf{F}, \hat{\Theta}\mathbf{G}) &= \int d^3\mathbf{r}\mathbf{F}^* \cdot \nabla \times \left(\frac{\mathbf{1}}{\varepsilon}\nabla \times \mathbf{G}\right) \\ &= \int d^3\mathbf{r}(\nabla \times \mathbf{F})^* \cdot \frac{\mathbf{1}}{\varepsilon}\nabla \times \mathbf{G} \\ &= \int d^3\mathbf{r}\left[\nabla \times \left(\frac{\mathbf{1}}{\varepsilon}\nabla \times \mathbf{F}\right)\right]^* \cdot \mathbf{G} = (\hat{\mathbf{\Theta}}\mathbf{F}, \mathbf{G})\end{aligned} \tag{3.14}$$

In performing the integrations by parts, we neglected the surface terms that involve the values of the fields at the boundaries of integration. This is because in all cases of interest, one of two things will be true: either the fields decay to zero at large distances, or the fields are periodic in the region of integration. In either case, the surface terms vanish.

3.3 General Properties of the Harmonic Modes

Having established that $\hat{\Theta}$ is Hermitian, we can now show that the eigenvalues must be real numbers. Suppose $\mathbf{H}(\mathbf{r})$ is an eigenvector of $\hat{\Theta}$ with eigenvalue $(/c)^2$. Take the inner product of the master equation 3.7 with $\mathbf{H}(\mathbf{r})$:

[a] In particular, we use the vector identity that $\nabla(\mathbf{F}\times\mathbf{G}) = (\nabla\times\mathbf{F})\cdot\mathbf{G} - \mathbf{F}\cdot(\nabla\times\mathbf{G})$. Integrating both sides and applying the divergence theorem, we find that $\mathbf{F}\cdot(\nabla\times\mathbf{G}) = (\nabla \times \mathbf{F}) \cdot \mathbf{G}$ plus a surface term, from the integral of $\nabla \cdot (\mathbf{F} \times \mathbf{G})$, that vanishes as described above.

$$\begin{aligned} \hat{\Theta}\mathbf{H}(\mathbf{r}) &= (\omega^2/c^2)\mathbf{H}(\mathbf{r}) \\ \Longrightarrow (\mathbf{H}, \hat{\Theta}\mathbf{H}) &= (\omega^2/c^2)(\mathbf{H}, \mathbf{H}) \\ \Longrightarrow (\mathbf{H}, \hat{\Theta}\mathbf{H})^* &= (\omega^2/c^2)^*(\mathbf{H}, \mathbf{H}) \end{aligned} \tag{3.15}$$

Because $\hat{\Theta}$ is Hermitian, we know that $(\mathbf{H}, \hat{\Theta}\mathbf{H}) = (\hat{\Theta}\mathbf{H}, \mathbf{H})$. Additionally, from the definition of the inner product we know that $(\mathbf{H}, \hat{\Xi}\mathbf{H}) = (\hat{\Xi}\mathbf{H}, \mathbf{H})^*$ for any operator Ξ. Using these two pieces of information, we continue:

$$\begin{aligned} (\mathbf{H}, \hat{\Theta}\mathbf{H})^* = (\omega^2/c^2)^*(\mathbf{H}, \mathbf{H}) = (\hat{\Theta}\mathbf{H}, \mathbf{H}) = (\omega^2/c^2)(\mathbf{H}, \mathbf{H}) \\ \Longrightarrow (\omega^2/c^2)^* = (\omega^2/c^2) \end{aligned} \tag{3.16}$$

It follows that $\omega^2 = (\omega^2)^*$, or that ω^2 is real. By a different argument, we can also show that ω^2 is always nonnegative for $\varepsilon > 0$. Set $\mathbf{F} = \mathbf{G} = \mathbf{H}$ in the middle equation of 3.14, to obtain

$$(\mathbf{H}, \mathbf{H}) \left(\frac{\omega}{c}\right)^2 (\mathbf{H}, \hat{\Theta}\mathbf{H}) = \int d^3\mathbf{r} \frac{1}{\varepsilon} |\nabla \times \mathbf{H}|^2 \tag{3.17}$$

Since $\varepsilon(\mathbf{r}) \geq 0$ everywhere, the integrand on the right-hand side is everywhere nonnegative. The operator $\hat{\Theta}$ is said to be positive semi-definite. Therefore all of the eigenvalues ω^2 are nonnegative, and ω is real.

In addition, the Hermiticity of $\hat{\Theta}$ forces any two harmonic modes $\mathbf{H}_1(\mathbf{r})$ and $\mathbf{H}_2(\mathbf{r})$ with different frequencies ω_1 and ω_2 to have an inner product of zero. Consider two normalized modes, $\mathbf{H}_1(\mathbf{r})$ and $\mathbf{H}_2(\mathbf{r})$, with frequencies ω_1 and ω_2:

$$\begin{aligned} \omega_1^2(\mathbf{H}_2, \mathbf{H}_1) = c^2(\mathbf{H}_2, \hat{\Theta}\mathbf{H}_1) = c^2(\hat{\Theta}\mathbf{H}_2, \mathbf{H}_1) = \omega_2^2(\mathbf{H}_2, \mathbf{H}_1) \\ \Longrightarrow (\omega_2^2 - \omega_1^2)(\mathbf{H}_2, \mathbf{H}_1) = 0 \end{aligned} \tag{3.18}$$

If $\omega_1 = \omega_2$, then we must have $(\mathbf{H}_1, \mathbf{H}_2) = 0$ and we say $\mathbf{H}_1$ and $\mathbf{H}_2$ are orthogonal modes. If two harmonic modes have equal frequencies $\omega_1 = \omega_2$, then we say they are degenerate and they are not necessarily orthogonal. For two modes to be degenerate requires to have precisely the same frequency: usually there is a symmetry that is responsible for the coincidence. For example, if the dielectric configuration is invariant under a 120 rotation, modes that differ only by a 120 rotation are expected to have the same frequency. Such modes are degenerate and are not necessarily orthogonal.

However, since $\hat{\Theta}$ is linear, any linear combination of these degenerate modes is itself a mode with that same frequency. As in quantum mechanics, we can always choose to work with linear combinations that are orthogonal. This allows us to say quite generally that different modes are orthogonal, or can be arranged to be orthogonal.

3.4 Magnetic vs. Electric Fields

The idea at the beginning of this chapter was that for a given frequency, we could solve for $\mathbf{H}(\mathbf{r})$ and then determine the $\mathbf{E}(\mathbf{r})$ via equation 3.8. But we could have equally well tried the alternate approach: solve for the electric field in 3.6 and then determine the magnetic field with 3.9.

By pursuing this alternate approach, one finds the condition on the electric field to be

$$\nabla \times \nabla \times \mathbf{E}(\mathbf{r}) = \left(\frac{\omega}{c}\right)^2 \varepsilon(\mathbf{r})\mathbf{E}(\mathbf{r}) \tag{3.19}$$

Because there are operators on both sides of this equation, it is referred to as a generalized eigenproblem. It is a simple matter to convert this into an ordinary eigenproblem by dividing 3.19 by ε, but then the operator is no longer Hermitian. If we stick to the generalized eigenproblem, however, then simple theorems analogous to those of the previous section can be developed because the two operators of the generalized eigenproblem, $\nabla \times \nabla \times$ and $\varepsilon(\mathbf{r})$, are easily shown to be both Hermitian

and positive semi-definite[b]. In particular, it can be shown that ω is real, and that two solutions $\mathbf{E_1}$ and $\mathbf{E_2}$ with different frequencies satisfy an orthogonality relation: $(\mathbf{E_1}, \varepsilon\mathbf{E_2}) = \mathbf{0}$.

The $\mathbf{E}$ eigenproblem has one feature that turns out to be undesirable for numerical computation: the transversality constraint $\nabla \cdot \varepsilon\mathbf{E} = 0$ depends on ε. We can restore a simpler transversality constraint by using $\mathbf{D}$ instead of $\mathbf{E}$, since $\nabla \cdot \mathbf{D} = 0$. Substituting $\mathbf{D}/\varepsilon_0\varepsilon$ for $\mathbf{E}$ in 3.19 and dividing both sides by ε (to keep the operator Hermitian) yields

$$\frac{1}{\varepsilon(\mathbf{r})}\nabla \times \nabla \times \frac{1}{\varepsilon(\mathbf{r})}\mathbf{D}(\mathbf{r}) = \left(\frac{w}{c}\right)^2 \frac{1}{\varepsilon(\mathbf{r})}\mathbf{D}(\mathbf{r}) \tag{3.20}$$

This is a perfectly valid formulation of the problem, but it seems unnecessarily complicated because of the three factors of $1/\varepsilon$ (as opposed to the single factor in the $\mathbf{H}$ or $\mathbf{E}$ formulations). For these reasons of mathematical convenience, we tend to prefer the $\mathbf{H}$ form for numerical calculations.

3.5 Scaling Properties of the Maxwell Equations

One interesting feature of electromagnetism in dielectric media is that there is no fundamental length scale other than the assumption that the system is macroscopic. In atomic physics, the spatial scale of the potential function is generally set by the fundamental length scale of the Bohr radius. Consequently, configurations of material that differ only in their overall spatial scale nevertheless have very different physical properties. For photonic crystals, there is no fundamental constant with the dimensions of length, since the master equation is scale invariant.

[b]The $\varepsilon(\mathbf{r})$ operator on the right-hand side is actually positive definite: $(\mathbf{E}, \varepsilon\mathbf{E})$ is strictly positive for any nonzero E. This is necessary for the generalized eigenproblem to be well behaved.

This leads to simple relationships between electromagnetic problems that differ only by a contraction or expansion of all distances.

Suppose, for example, we have an electromagnetic eigenmode $\mathbf{H}(\mathbf{r})$ of frequency ω in a dielectric configuration $\varepsilon(\mathbf{r})$. We recall the master equation 3.7:

$$\nabla \times \left(\frac{1}{\varepsilon}(\mathbf{r})\nabla \times \mathbf{H}(\mathbf{r})\right) = \left(\frac{\omega}{c}\right)^2 \mathbf{H}(\mathbf{r}) \tag{3.21}$$

Now suppose we want to calculate the harmonic modes in a configuration of dielectric $\varepsilon(\mathbf{r})$ that is just a compressed or expanded version of $\varepsilon(\mathbf{r}) : \varepsilon(\mathbf{r}) = \varepsilon(\mathbf{r}/s)$ for some scale parameter s. We make a change of variables in 3.21, using $\mathbf{r} = s\mathbf{r}$ and $\nabla = \nabla/s$:

$$s\nabla' \times \left(\frac{1}{\varepsilon}(\mathbf{r}'/s)s\nabla' \times \mathbf{H}(\mathbf{r}'/s)\right) = \left(\frac{\omega}{c}\right)^2 \mathbf{H}(\mathbf{r}'/s) \tag{3.22}$$

But $\varepsilon(\mathbf{r}'/s)$ is none other than $\varepsilon'(r')$. Dividing out the s's shows that

$$\nabla' \times \left(\frac{1}{\varepsilon}'(\mathbf{r}')\nabla' \times \mathbf{H}(\mathbf{r}'/s)\right) = \left(\frac{\omega}{c}s\right)^2 \mathbf{H}(\mathbf{r}'/s) \tag{3.23}$$

This is just the master equation again, this time with mode profile $\mathbf{H}'(\mathbf{r}') = \mathbf{H}(\mathbf{r}'/s)$ and frequency $\omega' = \omega/s$. What this means is that the new mode profile and its corresponding frequency can be obtained by simply rescaling the old mode profile and its frequency. The solution of the problem at one length scale determines the solutions at all other length scales.

This simple fact is of considerable practical importance. For example, the microfabrication of complex micron-scale photonic crystals can be quite difficult. But models can be easily made and tested in the microwave regime, at the much larger length scale of centimeters, if materials can be found that have nearly the same dielectric constant. The considerations in this section guarantee that the model will have the same electromagnetic properties.

3.6 Electrodynamics and quantum mechanics compared

For the benefit of those readers familiar with quantum mechanics, we now present some similarities between our formulation of electrodynamics in dielectric media and the quantum mechanics of noninteracting electrons.

	Quantum mechanics	Electrodynamics
Field	$\Psi(\mathbf{r},t) = \Psi(\mathbf{r})e^{-iEt/\hbar}$	$\mathbf{H}(\mathbf{r},t) = \mathbf{H}(\mathbf{r})e^{-i\omega t}$
Eigenvalue problem	$\hat{H}\Psi = E\Psi$	$\hat{\Theta}\mathbf{H} = \left(\frac{\omega}{c}\right)^2 \mathbf{H}$
Hermitian operator	$\hat{H} = -\frac{\hbar^2}{2m}\nabla^2 + V(\mathbf{r})$	$\Theta = \nabla \times \frac{1}{\varepsilon(\mathbf{r})}\nabla\times$

In both cases, we decompose the fields into harmonic modes that oscillate with a phase factor $e^{-i\omega t}$. In quantum mechanics, the wave function is a complex scalar field. In electrodynamics, the magnetic field is a real vector field and the complex exponential is just a mathematical convenience.

In both cases, the modes of the system are determined by a Hermitian eigenvalue equation. In quantum mechanics, the frequency ω is related to the eigenvalue via $\mathbf{E} = \hbar\omega$, which is meaningful only up to an overall additive constant V_0. In electrodynamics, the eigenvalue is proportional to the square of the frequency, and there is no arbitrary additive constant.

One difference we did not discuss, but is apparent from Table 3.6, is that in quantum mechanics, the Hamiltonian is separable if $V(\mathbf{r})$ is separable. For example, if $V(\mathbf{r})$ is the sum of one-dimensional functions $V_x(x) + V_y(y) + V_z(z)$, then we can write Ψ as a product $\Psi(\mathbf{r}) = X(x)Y(y)Z(z)$ and the problem separates into three more manageable

problems, one for each direction. In electrodynamics, such a factorization is not generally possible: the differential operator, $\hat{\Theta}$, couples the different coordinates even if $\varepsilon(\mathbf{r})$ is separable. This makes analytical solutions rare, and generally confined to very simple systems. To demonstrate most of the interesting phenomena associated with photonic crystals, we will usually make use of numerical solutions.

In quantum mechanics, the lowest eigenstates typically have the amplitude of the wave function concentrated in regions of low potential, while in electrodynamics the lowest modes have their electric-field energy concentrated in regions of high dielectric constant. Both of these statements are made quantitative by a variational theorem.

Finally, in quantum mechanics, there is usually a fundamental length scale that prevents us from relating solutions to potentials that differ by a scale factor. Electrodynamics is free from such a length scale, and the solutions we obtain are easily scaled up or down in length scale and frequency.

Chapter 4

Symmetries and Solid-State Electromagnetism

If a dielectric structure has a certain symmetry, then the symmetry offers a convenient way to categorize the electromagnetic modes of that system. In this chapter, we will investigate what various symmetries of a system can tell us about its electromagnetic modes. Translational symmetries (both discrete and continuous) are important because photonic crystals are periodic dielectrics, and because they provide a natural setting for the discussion of band gaps. Some of the terminology of solid-state physics is appropriate, and will be introduced. We will also investigate rotational, mirror, inversion, and time-reversal symmetries.

4.1 Using Symmetries to Classify Electromagnetic Modes

In both classical mechanics and quantum mechanics, the symmetries of a system allow one to make general statements about that system's behavior. Because of the mathematical analogy we pursued in the last chapter, it is not too surprising that Careful attention to symmetry in fact helps to understand the properties of electromagnetic systems. We will begin with a concrete example of a symmetry and the conclusion we may draw from it, and will then pass on to a more formal discussion of symmetries in electromagnetism.

Suppose we want to find the modes that are allowed in the two-

dimensional metal cavity shown in figure 1. Its shape is somewhat arbitrary, which would make it difficult to write down the exact boundary condition and solve the problem analytically. But the cavity has an important symmetry: if you invert the cavity about its center, you end up with exactly the same cavity shape. So if, somehow, we find that the particular pattern $\mathbf{H}(\mathbf{r})$ is a mode with frequency ω, then the pattern $\mathbf{H}(-\mathbf{r})$ must also be a mode with frequency ω. The cavity cannot distinguish between these two modes, since it cannot tell r from $-r$.

Recall from chapter 3 that different modes with the same frequency are said to be degenerate. Unless $\mathbf{H}(\mathbf{r})$ is a member of a degenerate family of modes, then if $\mathbf{H}(-\mathbf{r})$ has the same frequency it must be the same mode. It must be nothing more than a multiple of $\mathbf{H}(\mathbf{r})$: $\mathbf{H}(-\mathbf{r}) = \alpha\mathbf{H}(\mathbf{r})$. But what is α? If we invert the system twice, picking up another factor of α, then we return to the original function $\mathbf{H}(\mathbf{r})$. Therefore $\alpha^2\mathbf{H}(\mathbf{r}) = \mathbf{H}(\mathbf{r})$, and we see that $\alpha = 1$ or -1. A given nondegenerate mode must be one of two types: either it is invariant under inversion, $\mathbf{H}(-\mathbf{r}) = \mathbf{H}(\mathbf{r})$, and we call it even; or, it becomes its own opposite, $-\mathbf{H}(-\mathbf{r}) = \mathbf{H}(\mathbf{r})$, and we call it odd[a]. These possibilities are depicted in figure 4.1. We have classified the modes of the system based on how they respond to one of its symmetry operations.

With this example in mind, we can capture the essential idea in more abstract language. Suppose I is an operator (a 3×3 matrix) that inverts vectors (3×1 matrices), so that $I\mathbf{a} = \mathbf{a}$. To invert a vector field, we use an operator $\hat{O}_I$ that inverts both the vector $\mathbf{f}$ and its argument $\mathbf{r}$: $\hat{O}_I\mathbf{f}(\mathbf{r}) = I\mathbf{f}(I\mathbf{r})$. What is the mathematical expression of the statement that our system has inversion symmetry? Since inversion is a symmetry of our system, it does not matter whether we operate with $\hat{\Theta}$ or we first invert the coordinates, then operate with $\hat{\Theta}$, and then change them back:

[a]This is not automatically true of degenerate modes. But we can always form new modes that are even or odd, by taking appropriate linear combinations of the degenerate modes.

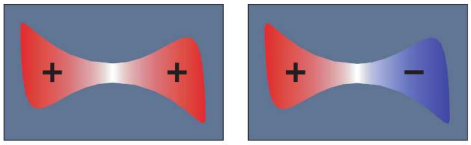

Figure 4.1: A two-dimensional metallic cavity with inversion symmetry. Red and blue suggest positive and negative fields. On the left, an even mode occupies the cavity, for which $\mathbf{H}(\mathbf{r}) = \mathbf{H}(-\mathbf{r})$. On the right, an odd mode occupies the cavity, for which $\mathbf{H}(\mathbf{r}) = -\mathbf{H}(-\mathbf{r})$.

$$\hat{\Theta} = \hat{O}_I^{-1}\hat{\Theta}\hat{O}_I \tag{4.1}$$

This equation can be rearranged as $\hat{O}_I\hat{\Theta} - \hat{\Theta}\hat{O}_I = 0$. Following this cue, we define the commutator $[\hat{A}, \hat{B}]$ of two operators $\hat{A}$ and $\hat{B}$ just like the commutator in quantum mechanics:

$$[\hat{A}, \hat{B}] \triangleq \hat{A}\hat{B} - \hat{B}\hat{A} \tag{4.2}$$

Note that the commutator is itself an operator. We have shown that our system is symmetric under inversion only if the inversion operator commutes with $\hat{\Theta}$; that is, we must have $[\hat{O}_I, \hat{\Theta}] = 0$. If we now operate with this commutator on any mode of the system $\mathbf{H}(\mathbf{r})$, we obtain

$$[\hat{O}_I, \hat{\Theta}]\mathbf{H} = \hat{O}_I(\hat{\Theta}\mathbf{H}) - \hat{\Theta}(\hat{O}_I\mathbf{H}) = 0 \Longrightarrow \hat{\Theta}(\hat{O}_I\mathbf{H}) = \hat{O}_I(\hat{\Theta}\mathbf{H}) = \frac{\omega^2}{c^2}(\hat{O}_I\mathbf{H}) \tag{4.3}$$

This equation tells us that if $\mathbf{H}$ is a harmonic mode with frequency ω, then $\hat{O}_I\mathbf{H}$ is also a mode with frequency ω. If there is no degeneracy, then there can only be one mode per frequency, so $\mathbf{H}$ and $\hat{O}_I\mathbf{H}$ can be different only by a multiplicative factor: $\hat{O}_I\mathbf{H} = \alpha\mathbf{H}$. But this is just the eigenvalue equation for $\hat{O}_I$, and we already know that the eigenvalues α must be either 1 or -1. Thus, we can classify the eigenvectors $\mathbf{H}(\mathbf{r})$

according to whether they are even ($\mathbf{H} \to +\mathbf{H}$) or odd ($\mathbf{H} \to -\mathbf{H}$) under the inversion symmetry operation $\hat{O}_I$.

Whenever two operators commute, one can construct simultaneous eigenfunctions of both operators. One reason why this is convenient is that eigenfunctions and eigenvalues of simple symmetry operators like $\hat{O}_I$ are easily determined, whereas those for $\hat{\Theta}$ are not. But if $\hat{\Theta}$ commutes with a symmetry operator $\hat{S}$, we can construct and catalogue the eigenfunctions of $\hat{S}$ properties. In the case of inversion symmetry, we can classify the $\hat{\Theta}$ eigenfunctions as either odd or even.

4.2 Continuous Translational Symmetry

Another symmetry that a system might have is continuous translation symmetry. Such a system is unchanged if we translate everything through the same distance in a certain direction. Given this information, we can determine the functional form of the system's modes.

A system with translational symmetry is unchanged by a translation through a displacement $\mathbf{d}$. For each $\mathbf{d}$, we can define a translation operator $\hat{T}_d$ which, when operating on a function $\mathbf{f}(\mathbf{r})$, shifts the argument by $\mathbf{d}$. Suppose our system is translationally invariant; then we have $\hat{T}_d\varepsilon(\mathbf{r}) = \varepsilon(\mathbf{r}-\mathbf{d}) = \varepsilon(\mathbf{r})$, or equivalently, $[\hat{T}_d, \hat{\Theta}] = 0$. The modes of $\hat{\Theta}$ can now be classified according to how they behave under $\hat{T}_d$.

A system with continuous translation symmetry in the z direction is invariant under all of the $\hat{T}_d$'s for that direction. We can prove that a mode with the functional form e^{ikz} is an eigenfunction of any translation operator in the z direction:

$$\hat{T}_d e^{ikz} = e^{ik(z-d)} = (e^{-ikd})e^{ikz} \tag{4.4}$$

The corresponding eigenvalue is e^{ikd}. With a little more work, one can show the converse, too: any eigenfunction of $\hat{T}_d$ for all $\mathbf{d} = d\hat{z}$ must be proportional to e^{ikz} for some k.[b]. The modes of our system can be

[b] If $f(x) \neq 0$ is such an eigenfunction, then $f(xd) = \lambda(d)f(x)$ for all d and some

chosen to be eigenfunctions of all the $\hat{T}_d$'s, so we therefore know they should have a z dependence of the functional form e^{ikz} (the z dependence is separable). We can classify them by the particular values for k, the wave vector. (k must be a real number in an infinite system where we require the modes to have bounded amplitudes at infinity.)

A system that has continuous translational symmetry in all three directions is a homogeneous medium: $\varepsilon(\mathbf{r})$ is a constant ε (= 1 for free space). Following a line of argument similar to the one above, we can deduce that the modes must have the form

$$\mathbf{H}_\mathbf{k}(\mathbf{r}) = \mathbf{H_0} e^{i\mathbf{k}\cdot\mathbf{r}} \tag{4.5}$$

where $\mathbf{H}_0$ is any constant vector. These are plane waves, polarized in the direction of $\mathbf{H}_0$. Imposing the transversality requirement (see equation 3.5 of chapter 3) gives the further restriction $\mathbf{k} \cdot \mathbf{H}_0 = 0$. The reader can also verify that these plane waves are in fact solutions of the master equation with eigenvalues $(\omega/c)^2 = |\mathbf{k}|^2/\varepsilon$, yielding the dispersion relation $\omega = c|\mathbf{k}|/\sqrt{\varepsilon}$. We classify a plane wave by its wave vector $\mathbf{k}$, which specifies how the mode is transformed by a continuous translation operation.

Another simple system with continuous translational symmetry is an infinite plane of dielectric material. In this case, the dielectric function varies in the z direction, but not in the x or y directions: $\varepsilon(\mathbf{r}) = \varepsilon(z)$. The system is invariant under all of the translation operators of the xy plane. We can classify the modes according to their in-plane wave vectors, $\mathbf{k} = k_x\hat{\mathbf{x}} + k_y\hat{\mathbf{y}}$. The x and y dependence must once again be a complex exponential (a plane wave):

$$\mathbf{H}_\mathbf{k}(\mathbf{r}) = e^{i\mathbf{k}\cdot\rho}\mathbf{h}(z) \tag{4.6}$$

The function $\mathbf{h}(z)$, which depends on k, cannot be determined in

eigenvalues $\lambda(d)$ Scale $f(x)$ so that $f(0) = 1$ and thus $f(x) = f(0[x]) = (x)$. Therefore, $f(x + y) = f(x)f(y)$, and the only anywhere-continuous functions with this property are $f(x) = e^{cx}$ for some constant c

the same way, because the system does not have translational symmetry in that direction. Althought the transversality condition implies one restriction on $\mathbf{h}$: substitution of 4.6 into $\nabla \cdot \mathbf{H}_k = 0$ gives $\mathbf{k} \cdot \mathbf{h} = i\partial h_z/\partial z$.)

The modes can be classified by their values of $\mathbf{k}$ and can be lined up in order of increasing frequency for a given value of $\mathbf{k}$. Let n, called the band number, stand for a particular mode's place in line of increasing frequency, so that we can identify any mode by its unique name $(\mathbf{k}, n)$. If there is degeneracy, then we might have to include an additional index to name the degenerate modes that have the same n and $\mathbf{k}$.

4.3 Discrete Translational Symmetry

Photonic crystals, like traditional crystals of atoms or molecules, do not have continuous translational symmetry. Instead, they have discrete translational symmetry. That is, they are not invariant under translations of any distance, but rather, only distances that are a multiple of some fixed step length.

The basic step length is the lattice constant a, and the basic step vector is called the primitive lattice vector $\mathbf{a} = a\hat{\mathbf{x}}_i$. Because of this discrete symmetry, $\varepsilon(\mathbf{r}) = \varepsilon(\mathbf{r} \pm \mathbf{a})$. By repeating this translation, we see that $\varepsilon(\mathbf{r}) = \varepsilon(\mathbf{r} + \mathbf{R})$ for any $\mathbf{R}$ that is an integral multiple of $\mathbf{a}$; that is, $\mathbf{R} = l\mathbf{a}$, where l is an integer. The dielectric unit that is repeated over and over is known as the unit cell.

For simplicity's sake let's examine the case of a one dimensional photonic crystal, repetitive only in the y direction. Because of the translational symmetries, $\hat{\Theta}$ must commute with all of the translation operators in the x direction, as well as the translation operators for lattice vectors $\mathbf{R} = la\hat{\mathbf{y}}$ in the y direction. With this knowledge, we can identify as simultaneous eigenfunctions of both translation operators. As the modes of $\hat{\Theta}$ before, these eigenfunctions are plane waves:

$$\begin{aligned}\hat{T}_{d\hat{\mathbf{x}}}e^{ik_x x} &= e^{ik_x(x-d)} = (e^{ik_x d})e^{ik_x x} \\ \hat{T}_{\mathbf{R}}e^{ik_y y} &= e^{ik_y(y-la)} = (e^{ik_y la})e^{ik_y y}\end{aligned} \tag{4.7}$$

Inserting two modes that differs for $2\pi/a$ into 4.7 shows that they have the same $\hat{T}_{\mathbf{R}}$ eigenvalues. In fact, all of the modes with wave vectors of the form $\mathbf{k}_y + m(2\pi/a)$, where m is an integer, form a degenerate set; they all have the same $\hat{T}_{\mathbf{R}}$ eigenvalue of $e^{i(k_y la)}$. Augmenting k_y by an integral multiple of $b = 2\pi/a$ leaves the state unchanged. We call $\mathbf{b} = b\hat{\mathbf{y}}$ the primitive reciprocal lattice vector.

Since any linear combination of these degenerate eigenfunctions is itself an eigenfunction with the same eigenvalue, we can take linear combinations of our original modes to put them in the form

$$\begin{aligned}\mathbf{H}_{k_x,k_y} &= e^{ik_x x}\sum_m \mathbf{c}_{k_y,m}(z)e^{i(k_y+mb)y} \\ &= e^{ik_x x}\cdot e^{ik_y y}\cdot\sum_m \mathbf{c}_{k_y,m}(z)e^{imby} \\ &= e^{ik_x x}\cdot e^{ik_y y}\cdot \mathbf{u}_{k_y}(y,z)\end{aligned} \tag{4.8}$$

where the $\mathbf{c}$'s are expansion coefficients to be determined by explicit solution, and $\mathbf{u}(y,z)$ is (by construction) a periodic function in y: by inspection of equation 4.8, we can verify that $\mathbf{u}(y+a,z) = \mathbf{u}(y,z)$.

The discrete periodicity in the y direction leads to a y dependence for $\mathbf{H}$ that is simply the product of a plane wave with a y-periodic function. We can think of it as a plane wave, as it would be in free space, but modulated by a periodic function because of the periodic lattice:

$$\mathbf{H}(\ldots,y,\ldots) \propto e^{ik_y y}\cdot\mathbf{u}_{k_y}(y,\ldots) \tag{4.9}$$

This result is commonly known as Bloch's theorem: in solid-state physics, the form of 4.9 is known as a Bloch state.[57] Bloch states with wave vectors that differ by integral multiples of $b = 2\pi/a$ are not different

from a physical point of view. Thus, the mode frequencies must also be periodic in $k_y : \omega(k_y) = \omega(k_y + mb)$. In fact, we need only consider k_y to exist in the range $\pi/a < k_y\pi/a$. This region of nonredundant values of k_y is called the Brillouin zone.

The modes of a three-dimensional periodic system are Bloch states that can be labelled by a Bloch wave vector $\mathbf{k} = k_1\mathbf{b}_1 + k_2\mathbf{b}_2 + k_3\mathbf{b}_3$ where k lies in the Brillouin zone. Each value of the wave vector k inside the Brillouin zone identifies an eigenstate of $\hat{\Theta}$ with frequency $\omega(\mathbf{k})$ and an eigenvector $\mathbf{H}_\mathbf{k}$ of the form

$$\mathbf{H}_\mathbf{k}(\mathbf{r}) = e^{i\mathbf{k}\cdot\mathbf{r}}\mathbf{u}_\mathbf{k}(\mathbf{r}) \tag{4.10}$$

where $\mathbf{u}_\mathbf{k}(\mathbf{r})$ is a periodic function on the lattice: $\mathbf{u}_\mathbf{k}(\mathbf{r}) = \mathbf{u}_\mathbf{k}(\mathbf{r} + \mathbf{R})$ for all lattice vectors $\mathbf{R}$.

4.4 Photonic Band Structures

All of the information about Bloch states described by equation 4.10 is given by the wave vector $\mathbf{k}$ and the periodic function $\mathbf{u}_\mathbf{k}(\mathbf{r})$. To solve for $\mathbf{u}_\mathbf{k}(\mathbf{r})$, we insert the Bloch state into the master equation 3.7 of chapter 3:

$$\begin{aligned}
\hat{\Theta}\mathbf{H}_\mathbf{k} &= (\omega(\mathbf{k})/c)^2\mathbf{H}_\mathbf{k} \\
\nabla \times \frac{1}{\varepsilon(\mathbf{r})}\nabla \times e^{i\mathbf{k}\cdot\mathbf{r}}\mathbf{u}_\mathbf{k}(\mathbf{r}) &= (\omega(\mathbf{k})/c)^2 e^{i\mathbf{k}\cdot\mathbf{r}}\mathbf{u}_\mathbf{k}(\mathbf{r}) \\
(i\mathbf{k} + \nabla) \times \frac{1}{\varepsilon(\mathbf{r})}(i\mathbf{k} + \nabla) \times \mathbf{u}_\mathbf{k}(\mathbf{r}) &= (\omega(\mathbf{k})/c)^2\mathbf{u}_\mathbf{k}(\mathbf{r}) \\
\hat{\Theta}_\mathbf{k}\mathbf{u}_\mathbf{k}(\mathbf{r}) &= (\omega(\mathbf{k})/c)^2\mathbf{u}_\mathbf{k}(\mathbf{r})
\end{aligned} \tag{4.11}$$

Here we have defined $\hat{\Theta}_\mathbf{k}$ as a new Hermitian operator that appears in this substitution and depends on k:

$$\hat{\Theta}_\mathbf{k} \triangleq (i\mathbf{k} + \nabla) \times \frac{1}{\varepsilon(\mathbf{r})}(i\mathbf{k} + \nabla). \tag{4.12}$$

The function $\mathbf{u}$ and the mode profiles are determined by the eigenvalue problem in the fourth equation of 4.12, subject to transversality $(i\mathbf{k} + \nabla) \cdot \mathbf{u_k} = 0$ and the periodicity condition

$$\mathbf{u_k}(\mathbf{r}) = \mathbf{u_k}(\mathbf{r} + \mathbf{R}). \tag{4.13}$$

Because of this periodic boundary condition, we can regard the eigenvalue problem as being restricted to a single unit cell of the photonic crystal, leading to a discrete spectrum of eigenvalues. The frequency of each band, for a given n, varies continuously as k varies and this allows us to describe the modes of a photonic crystal as a family of continuous functions, $\omega_n(\mathbf{k})$, indexed in order of increasing frequency by the band number. The information contained in these functions is called the *band structure* of the photonic crystal. Studying the band structure of a crystal supplies us with most of the information we need to predict its optical properties.

4.5 Mirror Symmetry and the Separation of Modes

Under certain conditions mirror reflection symmetry allows us to separate the eigenvalue equation for $\hat{\Theta}_\mathbf{k}$ in a photonic crystal into two separate equations, one for each field polarization. In one case $\mathbf{H_k}$ is perpendicular to the mirror plane and $\mathbf{E_k}$ is parallel; while in the other case, $\mathbf{H_k}$ is in the plane and $\mathbf{E_k}$ is perpendicular. This simplification is convenient, because it provides immediate information about the mode symmetries and also facilitates the numerical calculation of their frequencies.

Considering again a dielectric photonic crystal periodic only in the y direction, we focus our attention on the reflections M_x on the yz plane, where M_x changes $\hat{\mathbf{x}}$ to $-\hat{\mathbf{x}}$ and leaves $\hat{\mathbf{y}}$ and $\hat{\mathbf{z}}$ alone. Let's define a mirror reflection operator $\hat{O}_{M_x}$, which reflects a vector field by using M_x on both its input and its output:

$$\hat{O}_{M_x}\mathbf{f}(\mathbf{r}) = M_x\mathbf{f}(M_x\mathbf{r}) \tag{4.14}$$

Two applications of the mirror reflection operator restore any system to its original state, so the possible eigenvalues of $\hat{O}_{M_x}$ are $+1$ and -1. Because the dielectric is symmetric under a mirror reflection in the yz plane, $\hat{O}_{M_x}$ commutes with $\hat{\Theta}$: $[\hat{\Theta}, \hat{O}_{M_x}] = 0$. As before, if we operate on $\mathbf{H_k}$ with this commutator we can show that $\hat{O}_{M_x}\mathbf{H_k}$ is just the Bloch state with the reflected wave vector $M_x\mathbf{k}$:

$$\hat{O}_{M_x}\mathbf{H_k} = e^{i\phi}\mathbf{H}_{M_x\mathbf{k}} \tag{4.15}$$

Here, ϕ is an arbitrary phase. This relation does not restrict the reflection properties of $\mathbf{H}_k$ very much, unless $\mathbf{k}$ happens to be pointed in such a way that $M_x\mathbf{k} = \mathbf{k}$. When this is true, 4.15 becomes an eigenvalue problem and, using 4.14, we see that $\mathbf{H_k}$ must obey

$$\hat{O}_{M_x}\mathbf{H_k}(\mathbf{r}) = \pm\mathbf{H_k}(\mathbf{r}) = M_x\mathbf{H_k}(M_x\mathbf{k}) \tag{4.16}$$

The electric field $\mathbf{E_k}$ obeys a similar equation, so that both the electric and magnetic fields must be either even or odd under the $\hat{O}_{M_x}$ operation. But $M_x\mathbf{r} = \mathbf{r}$ for any $\mathbf{r}$ in our dielectric (taken in the two-dimensional yz plane). Therefore, since $\mathbf{E}$ transforms like a vector and $\mathbf{H}$ transforms like a pseudovector,[58] the only nonzero field components of an $\hat{O}_{M_x}$ even mode must be H_x, E_y , and E_z . The odd modes are described by the components E_x, H_y , and H_z.

In general, given a reflection M such that $[\hat{\Theta}, \hat{O}_M] = 0$, this separation of modes is only possible at $M\mathbf{r} = \mathbf{r}$ for $M\mathbf{k} = \mathbf{k}$. Note from 4.11 that $\hat{\Theta}_k$ and $\hat{O}_M$ will not commute unless $M\mathbf{k} = \mathbf{k}$. These conditions can always be met for two-dimensional photonic crystals. Two-dimensional crystals are periodic in a certain plane, but are uniform along an axis perpendicular to that plane. Calling that axis the z axis, we know that the operation $\hat{z} \rightarrow -\hat{z}$ is a symmetry of the crystal for any choice of origin. It also follows that $M_z\mathbf{k}_\parallel = \mathbf{k}_\parallel$ for all wave vectors $\mathbf{k}_\parallel$ in the two-dimensional Brillouin zone. Thus the modes of every two-dimensional

photonic crystal can be classified into two distinct polarizations: either (E_x, H_y, H_z) or (H_x, E_y, E_z). The former, in which the electric field is confined to the xy plane, are called transverse-electric (**TE**) modes. The latter, in which the magnetic field is confined to the xy plane, are called transverse-magnetic (**TM**) modes.

4.6 Time Reversal Symmetry

Another interesting feature of the photonic bands is the time reversal symmetry, that tells us that any photonic band structure has inversion symmetry even though the crystal structure does not have inversion symmetry. If we take the complex conjugate of the master equation for $\hat{\Theta}$ (equation 3.7 of chapter 3), and use the fact that the eigenvalues are real for lossless materials, we obtain

$$\begin{aligned} (\hat{\Theta}\mathbf{H}_{\mathbf{k}n})^* &= \frac{\omega_n^2(\mathbf{k})}{c^2}\mathbf{H}_{\mathbf{k}n}^* \\ \hat{\Theta}\mathbf{H}_{\mathbf{k}n}^* &= \frac{\omega_n^2(\mathbf{k})}{c^2}\mathbf{H}_{\mathbf{k}n}^* \end{aligned} \tag{4.17}$$

By this manipulation, we see that $\mathbf{H}_{\mathbf{k}n}^*$ satisfies the same equation as $\mathbf{H}_{\mathbf{k}n}$, with the very same eigenvalue. But from 4.10 we see that $\mathbf{H}_{\mathbf{k}n}^*$ is just a Bloch state at $-\mathbf{k}$. It follows that

$$\omega_n(\mathbf{k}) = \omega_n(-\mathbf{k}) \tag{4.18}$$

The above relation holds for all photonic crystals. The frequency bands have inversion symmetry even if the crystal does not. Taking the complex conjugate of $\mathbf{H}_{\mathbf{k}n}$ is equivalent to reversing the sign of time t in the Maxwell equations, as can be verified from equation 3.5 of chapter 3. For this reason, we say that 4.18 is a consequence of the time-reversal symmetry of the Maxwell equations.

4.7 Group Velocity and Equifrequency Surfaces

In the case of a homogeneous, isotropic medium, $\mathbf{k}$ is the direction in which the wave propagates, but this is not necessarily true in a periodic medium. Rather, the direction and the speed with which electromagnetic energy passes through the crystal are given by the group velocity $\mathbf{v}_g$, which is a function of both the band index n and the wave vector $\mathbf{k}$:

$$\mathbf{v}_{g,n}(\mathbf{k}) \triangleq \nabla_{\mathbf{k}}\omega_n \triangleq \frac{\partial\omega_n}{\partial k_x}\hat{\mathbf{x}} + \frac{\partial\omega_n}{\partial k_y}\hat{\mathbf{y}} + \frac{\partial\omega_n}{\partial k_z}\hat{\mathbf{z}} \tag{4.19}$$

where $\nabla_{\mathbf{k}}$ is the gradient with respect to $\mathbf{k}$.

The propagation direction and the group velocity vector are always normal to the Equifrequency Surface (EFS), which is a construction made in reciprocal space that consists in a surface connecting all the $k-$points with the same frequency ω.

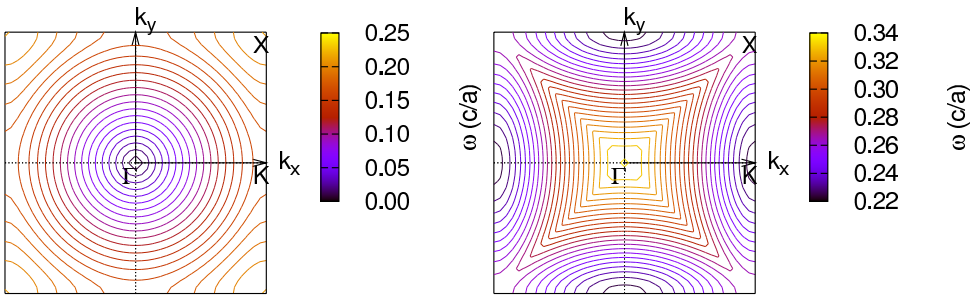

Figure 4.2: EFS plots for the TM modes of a square lattice of dielectric columns with $\varepsilon = 12$ in vacuum. On the left, the EFS radius increases with the frequency, because we are in the frequency range of the first band that rises from Γ with $\omega = 0$. On the right, the EFS radius shrinks with increasing frequency, indicating a negative gradient and thus a negative group velocity.

As an example, we show in figure 4.7 some equifrequency surfaces for the TM modes of a two-dimensional square lattice of dielectric columns ($\varepsilon = 12$) in vacuum in two different frequency ranges. We choose a 2D

case because it's simpler to visualize and because we will stick to 2D systems throughout this thesis.

In the left panel when the frequency grows, the radius of the EFS increases, meaning that the group velocity $\mathbf{v}_g$ is positive, while in the right panel the situation is reversed: a shrinking EFS radius with increasing frequency denotes negative group velocity.

Equifrequency surfaces are a usfeul tool to understand whether the group velocity is positive or negative and thus determine is negative refraction can happen.

4.8 Electrodynamics and Quantum Mechanics compared

Following the analogies with quantum mechanics underlined in chapter 3, in table 4.8 we compare the system containing an electron propagating in a periodic potential with the system of electromagnetic modes in a photonic crystal.

	Quantum mechanics	Electrodynamics
Discrete translational symmetry	$V(\mathbf{r}) = V(\mathbf{r}+\mathbf{R})$	$\varepsilon(\mathbf{r}) = \varepsilon(\mathbf{r}+\mathbf{R})$
Commutation relationships	$[\hat{H}, \hat{T}_{\mathbf{R}}]$	$[\hat{\Theta}, \hat{T}_{\mathbf{R}}]$
Bloch's theorem	$H_{\mathbf{k}n}(\mathbf{r}) = \mathbf{u}_{\mathbf{k}n}(\mathbf{r}) \cdot e^{i\mathbf{kr}}$	$\Psi_{\mathbf{k}n}(\mathbf{r}) = \mathbf{u}_{\mathbf{k}n}(\mathbf{r}) \cdot e^{i\mathbf{kr}}$

In both cases, the systems have translational symmetry: in quantum mechanics the potential $V(\mathbf{r})$ is periodic, and in the electromagnetic case the dielectric function $\varepsilon(\mathbf{r})$ is periodic. This periodicity implies that

the discrete translation operator commutes with the major differential operator of the problem, whether with the Hamiltonian or with $\hat{\Theta}$.

Using the translation operator eigenvalues we can index the eigenstates ($\Psi_{\mathbf{k}n}$ or $H_{\mathbf{k}n}$) and be label them in terms of the wave vectors and bands in the Brillouin zone. All of the eigenstates can be cast in Bloch form: a periodic function modulated by a plane wave. The field can propagate through the crystal in a coherent manner, as a Bloch wave. In the same way electrons behave like free particles in of conducting crystals, a photonic crystal provides a synthetic medium in which light can propagate, but in ways quite different from propagation in a homogeneous medium.

Chapter 5

Calculating Photonic Bands

5.1 Plane-wave Expansion

Because of the spatial periodicity of $\varepsilon(\mathbf{r}) = \varepsilon(\mathbf{r}+\mathbf{R})$, we can expand $\varepsilon^{-1}(\mathbf{r})$ in a Fourier series. Introducing the reciprocal lattice vectors $\mathbf{G}$:

$$\mathbf{G} = m_1\mathbf{b}_1 + m_2\mathbf{b}_2 + m_3\mathbf{b}_3 \tag{5.1}$$

where m_i are arbitrary integers. $\varepsilon^{-1}(\mathbf{r})$ is expressed as

$$\frac{1}{\varepsilon(\mathbf{r})} = \sum_{\mathbf{G}} \kappa(\mathbf{G}) e^{i\mathbf{G}\cdot\mathbf{r}} \tag{5.2}$$

and because we assumed that the dielectric function is real, $\kappa(-\mathbf{G})\kappa^*(\mathbf{G})$. From 4.10 we know that also $\mathbf{H}_\mathbf{k}(\mathbf{r}$ is periodic in space, so it can be expanded in Fourier series too, leading to the following form of the eigenfunction

$$\mathbf{H}_{\mathbf{k}n}(\mathbf{r}) = \sum_{\mathbf{G}} \mathbf{H}_{\mathbf{k}n}(\mathbf{G}) e^{i\mathbf{k}+\mathbf{G}\cdot\mathbf{r}}. \tag{5.3}$$

Substituting 5.2 and 5.3 into 3.7, we obtain the following eigenvalue equations for the expansion coefficient $\mathbf{H}_\mathbf{k}(\mathbf{G})$:

$$-\sum_{\mathbf{G}'} \kappa(\mathbf{G}-\mathbf{G}')(\mathbf{k}+\mathbf{G}) \times [(\mathbf{k}+\mathbf{G}') \times \mathbf{H}_{\mathbf{k}n}(\mathbf{G}')] = \frac{\omega_n^2(\mathbf{k})}{c^2} \mathbf{H}_{\mathbf{k}n}(\mathbf{G}). \tag{5.4}$$

By solving these equation numerically, we can obtain the dispersion realtion of the eigenmodes, or the photonic band structure.[59]

This numerical method, which is based on the Fourier expansion of the electromagnetic field and the dielectric function, is called the plane-wave expansion method. In the actual numerical calculation of the photonic bands, the summation in 5.4 is calculated up to a sufficiently large number of N of $\mathbf{G}'$, and an eigenvalue problem for each $\mathbf{k}$ is solved, which is equivalent to the diagonalization of the matrix defined by the left hand side of 5.4. The dimension of the matrix that should be diagonalized is $2N$ for $\mathbf{H}_{\mathbf{k}n}(\mathbf{G})$, since $\mathbf{H}_{\mathbf{k}n}$ should be perpendicular to $\mathbf{k}+\mathbf{G}$ according to 3.3 and 5.3, and its degree of freedom is two.

The CPU time that is necessary for the diagonalization is usually proportional to to the cube of its dimension. Hence, the CPU time for photonic band calculation by means of the plane-wave expansion method is proportional to N^3. This fact can lead to convergence problems in case of 3D systems or complex 2D systems such as photonic quasicrystals, where a supercell is needed. To overcome this issue several solutions were proposed.[60–64]

Because $\mathbf{H}_{\mathbf{k}}(\mathbf{G})$ is perpendicular to $\mathbf{k}+\mathbf{G}$, it can be expressed by a linear combination of two orthogonal normal vectors,[65] $e_{\mathbf{G}_1}$ and $e_{\mathbf{G}_2}$:

$$\mathbf{H}_{\mathbf{k}n}(\mathbf{G}) = h_{\mathbf{k}n}^{\mathbf{G}_1} e_{\mathbf{G}_1} + h_{\mathbf{k}n}^{\mathbf{G}_2} e_{\mathbf{G}_2}. \tag{5.5}$$

We assume without loss of generality that

$$\left\{ e_{\mathbf{G}_1}, e_{\mathbf{G}_2}, \frac{\mathbf{k}+\mathbf{G}}{|\mathbf{k}+\mathbf{G}|} \right\} \tag{5.6}$$

constitute a right-hand system. From 5.4 we derive the following equation:

$$\sum_{\mathbf{G}'} \sum_{j=1}^{2} \Lambda_{\mathbf{k}}^{ij}(\mathbf{G},\mathbf{G}') h_{\mathbf{k}n}^{\mathbf{G}'_j} = \frac{\omega_n^2(\mathbf{k})}{c^2} h_{\mathbf{k}n}^{\mathbf{G}'_i} \tag{5.7}$$

where $\Lambda_{\mathbf{k}}(\mathbf{G},\mathbf{G}')$ is given by

$$\Lambda_{\mathbf{k}}(\mathbf{G},\mathbf{G}') = |\mathbf{k}+\mathbf{G}||\mathbf{k}+\mathbf{G}'|\kappa(\mathbf{G}-\mathbf{G}') \times \begin{pmatrix} e_{\mathbf{G}_2}\cdot e_{\mathbf{G}'_2}, & -e_{\mathbf{G}_2}\cdot e_{\mathbf{G}'_1} \\ e_{\mathbf{G}_2}\cdot -e_{\mathbf{G}'_1}, & e_{\mathbf{G}_1}\cdot e_{\mathbf{G}'_1} \end{pmatrix} \tag{5.8}$$

which is an Hermitian matrix:

$$\Lambda^{ij}_{\mathbf{k}}(\mathbf{G},\mathbf{G}') = \Lambda^{ij*}_{\mathbf{k}}(\mathbf{G}',\mathbf{G}). \tag{5.9}$$

The eigenvectors $h_{\mathbf{k}}$ are thus orthogonal to each other:

$$\sum_{\mathbf{G}'}\sum_{i=1}^{2} h^{\mathbf{G}_i *}_{\mathbf{k}n}\cdot h^{\mathbf{G}_i}_{\mathbf{k}n'} = \delta_{nn'} \tag{5.10}$$

where δ_{ij} is the Kronecker delta. From this equation we obtain

$$\begin{aligned} &\int_V d\mathbf{r}\mathbf{H}^*_{\mathbf{k}n}(\mathbf{r})\cdot\mathbf{H}_{\mathbf{k}n'}(\mathbf{r}) \\ &= \int_V d\mathbf{r}\sum_{\mathbf{G}}{\sum_{\mathbf{G}}}' \mathbf{H}^*_{\mathbf{k}n}(\mathbf{G})\cdot\mathbf{H}_{\mathbf{k}n'}(\mathbf{G}')e^{i(\mathbf{G}'-\mathbf{G})\cdot\mathbf{r}} \\ &= \sum_{\mathbf{G}}\mathbf{H}^*_{\mathbf{k}n}(\mathbf{G})\cdot\mathbf{H}_{\mathbf{k}n'}(\mathbf{G}) \\ &= V\delta_{nn'}, \end{aligned} \tag{5.11}$$

where V denotes the volume of the photonic crystal. On the other hand, if $\mathbf{k}\neq\mathbf{k}'$,

$$\int_V d\mathbf{r}\mathbf{H}^*_{\mathbf{k}n}(\mathbf{r})\cdot\mathbf{H}_{\mathbf{k}'n'}(\mathbf{r}) = \int_V d\mathbf{r}\mathbf{v}^*_{\mathbf{k}n}(\mathbf{r})\cdot\mathbf{v}_{\mathbf{k}'n'}(\mathbf{r})e^{i(\mathbf{k}'-\mathbf{k})\cdot\mathbf{r}}. \tag{5.12}$$

Because both $\mathbf{k}$ and $\mathbf{k}'$ are wave vectors in the first brillouin zone, $\mathbf{k}'-\mathbf{k}$ cannot coincide with a reciprocal lattice vector. The periodicity of the function $\mathbf{v}^*_{\mathbf{k}n}(\mathbf{r})\cdot\mathbf{v}_{\mathbf{k}'n'}(\mathbf{r})$ thus lead to the above integral vanishing. Hence, we finally obtain

$$\int_V d\mathbf{r}\mathbf{H}^*_{\mathbf{k}n}(\mathbf{r}) \cdot \mathbf{H}_{\mathbf{k}'n'}(\mathbf{r}) = V\delta_{\mathbf{k}\mathbf{k}'}\delta_{nn'}. \tag{5.13}$$

This orthogonality is a direct consequence of the fact that the matrix $\Lambda_{\mathbf{k}}$ defined by 5.8 is Hermitian. The latter is, on the other hand, a consequence of the fact that $\hat{\Theta}$ defined by 3.7 is an Hermitian operator.

5.2 MIT Photonic Bands

The program used to calculate the photonic bands throughout this thesis is the MIT Photonic Bands (MPB) code,[64] which is available as a free and flexible computer program downloadable from the Web.[66]

This method can described as a fully-vectorial, three-dimensional method for computing general eigenmodes of arbitrary periodic dielectric systems, including anisotropy, based on the preconditioned block-iterative solution of Maxwells equations in a planewave basis. An effective dielectric tensor for anisotropic systems is introduced.

The approach is to expand the fields as definite-frequency states in some truncation of a complete basis (e.g. planewaves with a finite cutoff) and then solve the resulting linear eigenproblem.

The choice[60,62,67–70] is to use a planewave basis $|b_m\rangle$ in the form of 5.3 $|b_m\rangle = e^{i\mathbf{G}_m\cdot\mathbf{r}}$ for some reciprocal-lattice vectors $\mathbf{G}_m$; the truncation N is determined by choosing a maximum cutoff for the magnitude of $\mathbf{G}_m$. Strictly speaking, a cutoff magnitude would result in a spherical volume of $\mathbf{G}$ vectors, but the method expands this into a parallelopiped volume so that the transformation between planewave and spatial representations takes the convenient form of a Discrete Fourier Transform (DFT). (Such an extension also removes an ambiguity of the order in which to invert and Fourier-transform ε.[67,68]) The planewave set then has a duality with a spatial grid, which is often a more intuitive representation. The basis functions are:

$$|b_{m_1,m_2,m_3}\rangle = e^{i\sum_j m_j \mathbf{G}_j \cdot \mathbf{r}} \tag{5.14}$$

with $m_j = [N_j/2]+1, \cdots, [N_j/2], N = N_1N_2N_3$, and the equation 5.3 for the spatial field becomes:

$$\begin{aligned}\mathbf{H_k}\left(\sum_k n_k \mathbf{R}_k/N_k\right) &= \sum_{\{m_j\}} \mathbf{h}_{\{m_j\}} e^{i\sum_{j,k} m_j \mathbf{G}_j \cdot n_k \mathbf{R}_k/N_k} \\ &= \sum_{\{m_j\}} \mathbf{h}_{\{m_j\}} e^{2\pi i \sum_j m_j n_j/N_j}.\end{aligned} \tag{5.15}$$

Here, $n_k = 0, \cdots, N_k - 1$ describe spatial coordinates on an $N_1 \times N_2 \times N_3$ affine grid along the lattice directions. This is precisely a three-dimensional DFT, and can be computed by an efficient Fast Fourier Transform (FFT) algorithm[71] in $O(N \log N)$ time.

Thus, in a planewave representation, the product $\hat{\Theta}\mathbf{H}(\mathbf{r})$ from equation 3.10 can be computed in $O(N \log N)$ time by taking the curl in wavevector space (just the cross-product with $\mathbf{k} + \mathbf{G}_m$), computing the FFT, multipling by $\widetilde{\varepsilon^{-1}}$, computing the inverse FFT, and taking the curl again.[67,68]

5.3 The Effective Dielectric Tensor

When computing the product $\hat{\Theta}\mathbf{H}(\mathbf{r})$ in a planewave basis, the multiplication by $\varepsilon^{-1}(\mathbf{r})$ is done in the spatial domain after a Fourier transform, so one might simply use the inverse of the actual dielectric constant at that point.

To calculate the band structure for a simple 2D system such an approach is feasible,[72] writing the Fourier coefficient $\kappa(\mathbf{G}_\parallel)$ of 5.8 in the form:[73]

$$\kappa(\mathbf{G}_\parallel) = \begin{cases} \frac{1}{\varepsilon_a} f + \frac{1}{\varepsilon_b}(1-f), & \mathbf{G}_\parallel = 0 \\ \left(\frac{1}{\varepsilon_a} - \frac{1}{\varepsilon_b}\right) \frac{1}{a\,c} \int_A d^2\mathbf{r}_\parallel e^{-i\mathbf{G}_\parallel \cdot \mathbf{x}_\parallel}, & \mathbf{G}_\parallel \neq 0 \end{cases} \tag{5.16}$$

where f is the filling fraction of a dielectric medium ε_a embedded in another dielectric ε_b, defined as $f = a_A/a_c$, and a_A is the area of the domain A (i.e. the cross-sectional area) over the area of the 2D unit cell a_c.

Unfortunately, this can lead to suboptimal convergence of the frequencies as a function of N, due to the problems of representing discontinuities in a Fourier basis. It has been shown, however, that using a smoothed, effective dielectric tensor near dielectric interfaces can circumvent these problems, and achieve accurate results for moderate N.[67,68] In particular, near a dielectric interface, one must average the dielectric in two different ways according to effective-medium theory, depending upon the polarization of the incident light relative to the surface normal $\hat{n}$. For an electric field $\mathbf{E} \parallel \hat{n}$, one averages the inverse of ε while for $\mathbf{E} \perp \hat{n}$, one takes the inverse of the average of ε. This results in an effective dielectric tensor $\widetilde{\varepsilon^{-1}}$:

$$\widetilde{\varepsilon^{-1}} = \overline{\varepsilon^{-1}} P + \overline{\varepsilon}^{-1}(1 - P) \tag{5.17}$$

where is the projection matrix onto $\hat{n}$: $P_{ik} = n_i n_j$. Here, the averaging is done over one voxel (cubic unit grid) around the given spatial point: if ε is constant, equation 5.17 simply reduces to ε^{-1}.

5.4 Preconditioner and Iterative Eigensolver

We won't describe in detail the choice of neither the preconditioner nor the iterative eigensolver, for an exhaustive discussion we suggest reading the article where the MPB code is presented.[64] The basic idea is to use a preconditioning operator to improve the performance of the iterative eigensolver: the requirement is to supply an approximate inverse $\tilde{\Theta}^{-1}$ of $\hat{\Theta}$ such that $\tilde{\Theta}^{-1}\mathbf{h}$ can be computed quickly.

The iterative eigeinsolver used is an extension[74] of the conjugate-gradient Rayleigh-quotient method, that solves for all of the eigenvalues at once. The Rayleigh quotient is the variational problem minimized

by the smallest eigenvalue λ_0 and the corresponding eigenvector y_0 of a Hermitian matrix A:

$$\lambda_0 = \min \frac{y_0^\dagger A y_0}{y_0^\dagger B y_0} \tag{5.18}$$

where † denotes the conjugate transpose.

5.5 Complementary Method: Finite Difference Time Domain

In addition to the plane-wave expansion method we also perform calculations with a Finite Difference Time Domain (FDTD) code that can act as a simulated experiment and offer an immediate picture of the time evolution of a system in presence of an electromagnetic source.

FDTD is a widely used technique in which space is divided into a discrete grid and then the fields are evolved in time using discrete time steps. As the grid and the time steps are made finer and finer, this becomes a closer and closer approximation for the true continuous equations, and one can simulate many practical problems essentially exactly.[75]

The time-dependent Maxwell's equations in partial differential form:

$$\begin{aligned} \frac{\partial \mathbf{B}}{\partial t} &= -\nabla \times \mathbf{E} - \mathbf{J}_B - \sigma_B \mathbf{B} \quad \mathbf{B} = \mu \mathbf{H} \\ \frac{\partial \mathbf{D}}{\partial t} &= \nabla \times \mathbf{H} - \mathbf{J} - \sigma_D \mathbf{D} \quad \mathbf{D} = \varepsilon \mathbf{E} \end{aligned} \tag{5.19}$$

are discretized using central-difference approximations to the space and time partial derivatives. The resulting finite-difference equations

$$\begin{aligned} \nabla \cdot \mathbf{B} &= -\int^t \nabla \cdot (\mathbf{J}_B(t') + \sigma_B \mathbf{B}) dt' \\ \nabla \cdot \mathbf{D} &= -\int^t \nabla \cdot (\mathbf{J}(t') + \sigma_D \mathbf{D}) dt' = \rho \end{aligned} \tag{5.20}$$

are solved in either software or hardware in a leapfrog manner: the electric field vector components in a volume of space are solved at a given instant in time; then the magnetic field vector components in the same spatial volume are solved at the next instant in time and the process is repeated over and over again until the desired transient or steady-state electromagnetic field behavior is fully evolved.[76]

All the simulations we will show were performed using a freely available FDTD software package with subpixel smoothing for increased accuracy[77] using open boundary conditions.

To simulate open boundary conditions, one would like the boundaries to absorb all waves incident on them, with no reflections. This is implemented with something called perfectly matched layers (PML).[78] PML is, strictly speaking, not a boundary condition: rather, it is a special absorbing material placed adjacent to the boundaries. PML is actually a fictitious (non-physical) material, designed to have zero reflections at its interface. Although PML is reflectionless in the theoretical continous system, in the actual discretized system it has some small reflections which make it imperfect. For this reason, one always gives the PML some finite thickness in which the absorption gradually turns on.

With this additional tool we can have some first confirmations to any hypotesis we are extracting from the dispersion curves or the equifrequancy surfaces obtained with the plane-wave expansion code.

Chapter 6
Two-Dimensional Photonic Crystals

When the crystal is periodic in two directions and homogeneous in the third, photonic band gaps appear in the plane of periodicity. For light propagating in this plane, the harmonic modes can be divided into two independent polarizations, each with its own band structure. We will see also how the presence of defects gives rise to light modes localized in two dimensions.

6.1 Two-Dimensional Bloch States

A two-dimensional photonic crystal is periodic along two of its axes and homogeneous along the third axis, since we imagine the entire structure to be infinitely tall. For certain values of the lattice constant, a frequency range where no electromagnetic eigenmode exists can appear. Frequency ranges of this kind are called *photonic bandgaps*: in this case, a 2-D photonic crystal can have a photonic band gap in the xy plane. That means that inside this gap, no extended states are permitted, and incident light is reflected.

As always, we can use the symmetries of the crystal to characterize its electromagnetic modes. Because the system is homogeneous in the z direction, we know that the modes must be oscillatory in that direction, with no restrictions on the wave vector k_z . In addition, the system has discrete translational symmetry in the xy plane. Specifically, $\varepsilon(\mathbf{r}) = \varepsilon(\mathbf{r} + \mathbf{R})$, as long as $\mathbf{R}$ is any linear combination of the primitive lattice vectors $a\hat{\mathbf{x}}$ and $a\hat{\mathbf{y}}$. By applying Bloch's theorem, we can focus our

attention on the values of $\mathbf{k}_\parallel$ that are in the Brillouin zone. As before, we use the label n (band number) to label the modes in order of increasing frequency.

Indexing the modes of the crystal by $k_z, \mathbf{k}_\parallel$, and n, they take the form of Bloch states

$$\mathbf{H}_{k_z,\mathbf{k}_\parallel,n}(\mathbf{r}) = e^{i\mathbf{k}_\parallel\cdot\mathbf{r}_\parallel} e^{ik_z z} \mathbf{u}_{k_z,\mathbf{k}_\parallel,n}(\mathbf{r}_\parallel) \tag{6.1}$$

In this equation, $\mathbf{r}_\parallel$ is the projection of $\mathbf{r}$ in the xy plane and $\mathbf{u}(\mathbf{r}_\parallel)$ is a periodic function, $\mathbf{u}(\mathbf{r}_\parallel) = \mathbf{u}(\mathbf{r}_\parallel + \mathbf{R})$, for all lattice vectors $\mathbf{R}$. The parallel wavevector $\mathbf{k}_\parallel$ is periodic in the xy plane and restricted to the Brillouin zone and k_z is unrestricted.

Any modes with $k_z = 0$ (i.e. that propagate strictly parallel to the xy plane) are invariant under reflections through the xy plane. As discussed in chapter 4, this mirror symmetry allows us to classify the modes by separating them into two distinct polarizations. Transverse-electric (TE) modes have $\mathbf{H}$ normal to the plane, $\mathbf{H} = H(\mathbf{r}_\parallel)\hat{\mathbf{z}}$, and $\mathbf{E}$ in the plane, $\mathbf{E}(\mathbf{r}_\parallel)\cdot\hat{\mathbf{z}} = 0$. Transverse-magnetic (TM) modes have just the reverse: $\mathbf{E} = E(\mathbf{r}_\parallel)\hat{\mathbf{z}}$ and $\mathbf{H}(\mathbf{r}_\parallel)\cdot\hat{\mathbf{z}} = 0$.

The band structures for TE and TM modes can be completely different. It is possible, for example, that there are photonic band gaps for one polarization but not for the other polarization.

For the TE case, the maxwell equations 3.3 simplify to:

$$\frac{\partial}{\partial y} H_z(\mathbf{r}_\parallel, t) = \varepsilon_0 \varepsilon(\mathbf{r}_\parallel) \frac{\partial}{\partial t} E_x(\mathbf{r}_\parallel, t) \tag{6.2}$$

$$\frac{\partial}{\partial x} H_z(\mathbf{r}_\parallel, t) = -\varepsilon_0 \varepsilon(\mathbf{r}_\parallel) \frac{\partial}{\partial t} E_y(\mathbf{r}_\parallel, t) \tag{6.3}$$

$$\frac{\partial}{\partial x} E_y(\mathbf{r}_\parallel, t) - \frac{\partial}{\partial y} E_x(\mathbf{r}_\parallel, t) = -\mu_0(\mathbf{r}_\parallel) \frac{\partial}{\partial t} H_z(\mathbf{r}_\parallel, t) \tag{6.4}$$

eliminating E_x and E_y we obtain the wave equation for $H_z(\mathbf{r}_\parallel, t)$:

$$\hat{\Theta}^{(2)}\mathbf{H}_z(\mathbf{r}_\parallel) \triangleq -\left\{\frac{\partial}{\partial x}\frac{1}{\varepsilon(\mathbf{r}_\parallel)}\frac{\partial}{\partial x} + \frac{\partial}{\partial y}\frac{1}{\varepsilon(\mathbf{r}_\parallel)}\frac{\partial}{\partial y}\right\}\mathbf{H}_z(\mathbf{r}_\parallel) = \frac{\omega^2}{c^2}\mathbf{H}_z(\mathbf{r}_\parallel) \tag{6.5}$$

where the differential operator $\hat{\Theta}^{(2)}$ for the 2D case is defined by the first equality in the above equation.

Substituting 6.1 into 6.5, we obtain the following eigenvalue equations for the expansion coefficients:[73]

$$\sum_{\mathbf{G}'_\parallel} \kappa(\mathbf{G}_\parallel - \mathbf{G}'_\parallel)(\mathbf{k}_\parallel - \mathbf{G}_\parallel)\cdot(\mathbf{k}_\parallel - \mathbf{G}'_\parallel)H_{z,\mathbf{k}_\parallel n}(\mathbf{G}'_\parallel) = \frac{\omega_n^2(\mathbf{k}_\parallel)}{c^2}H_{z,\mathbf{k}_\parallel n}(\mathbf{G}_\parallel). \tag{6.6}$$

If we define a matrix $\Lambda_{\mathbf{k}_\parallel}$ as we did in 5.7

$$\Lambda_{\mathbf{k}_\parallel}(\mathbf{G}_\parallel, \mathbf{G'}_\parallel)\kappa(\mathbf{G}_\parallel - \mathbf{G}'_\parallel)(\mathbf{k}_\parallel - \mathbf{G}_\parallel)\cdot(\mathbf{k}_\parallel - \mathbf{G}'_\parallel), \tag{6.7}$$

we see it is Hermitian:

$$\Lambda_{\mathbf{k}_\parallel}(\mathbf{G}_\parallel, \mathbf{G'}_\parallel) = \Lambda^*_{\mathbf{k}_\parallel}(\mathbf{G'}_\parallel, \mathbf{G}_\parallel). \tag{6.8}$$

The eigenvalue equation 6.6 is thus expressed as

$$\sum_{\mathbf{G}'_\parallel} \Lambda_{\mathbf{k}_\parallel}(\mathbf{G}_\parallel, \mathbf{G'}_\parallel)H_{z,\mathbf{k}_\parallel n}(\mathbf{G}'_\parallel) = \frac{\omega_n^2(\mathbf{k}_\parallel)}{c^2}H_{z,\mathbf{k}_\parallel n}(\mathbf{G}_\parallel). \tag{6.9}$$

As we derived the orthogonality of $\mathbf{H}_{\mathbf{k}n}(\mathbf{r})$ in 5.13, we can prove that

$$\int_{V^{(2)}} d\mathbf{r}_\parallel H^*_{z,\mathbf{k}_\parallel n}(\mathbf{r}_\parallel)H_{z,\mathbf{k}'_\parallel n'}(\mathbf{r}_\parallel) = V^{(2)}\delta_{\mathbf{k}_\parallel \mathbf{k}'_\parallel}\delta_{nn'}, \tag{6.10}$$

where $V^{(2)}$ denotes the 2D volume of the photonic crystal. This orthogonality relation is a consequence of the fact that $\hat{\Theta}^{(2)}$ is a Hermitian operator.

6.2 2D Square Lattice of Dielectric Rods in Air

Consider light that propagates in the xy plane of a square array of dielectric columns, such as the structure depicted in figure 6.1, with lattice constant a. The band structure for a crystal of dielectric ($\varepsilon = 12$) rods in air, with radius $r/a = 0.2$, is plotted in figure 6.2. The calculations were made using the MPB code[64] described in chapter 5.

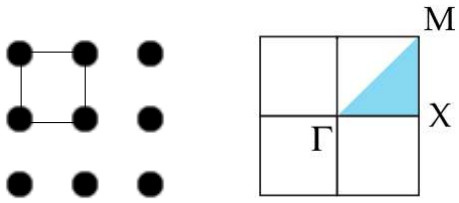

Figure 6.1: On the left, a cross-sectional view of the dielectric function of the 2D square photonic crystal; on the right, the corresponding 2D Brillouin Zone, with the irreducible zone highlighted and delimited by high symmetry points.

Both the TE and the TM band structures are shown, with the frequency expressed as a function of the ratio c/a, since the problem is scalable as discussed in section 3.5. The abscissa shows the value of the in-plane wave vector $\mathbf{k}_{\|}$. As we move from left to right, $\mathbf{k}_{\|}$ moves along the triangular edge of the irreducible Brillouin zone, from Γ to X to M and back to Γ, as shown in figure 6.1.

As we can see, the TM dispersion curves show a photonic bandgap over the entire Brillouin zone between the first and second band, while the TE modes don't have any complete bandgap.

To get an insight of the behaviour of electromagnetic fields inside the structure, it can also be useful to visualize the field distribution for both the electric and magnetic field.

Figure 6.2 show the electric field distribution for the first three bands of the TM dispersion curves seen in fig. 6.2 taken at k-point M. As before, the image show a cross-sectional view of the two-dimensional system, so the color indicates the intensity of the electric field in the z direction

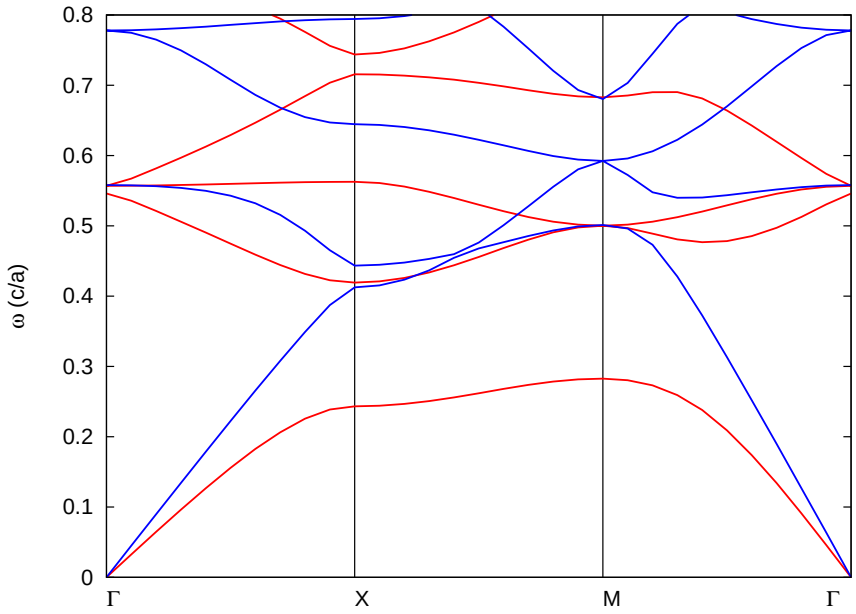

Figure 6.2: Photonic band structure for a 2D PC with dielectric rods in a square lattice. The rods have dieletric constant of $\varepsilon = 12$ and radius $r = 0.2a$. Red bands are TM modes and blue bands are TE modes. Frequencies ω are expressed as dimensionless unit c/a and must be scaled to the corresponding lattice constant a to obtain experimental frequency in Hz. TM modes presents two photonic gaps while TE modes have none. Calculation made with MPB.[64]

perpendicular to the page plane. White means zero field intensity, so white areas are nodal planes for the modes. Figure 6.2 shows instead the magnetic field distribution for the same system.

6.3 2D Hexagonal Lattice of air Holes in a Dielectric Matrix

We focus our attention now to another system, a triangular lattice of air columns in a dielectric matrix of $\varepsilon = 12$. The columns have radius 0.45

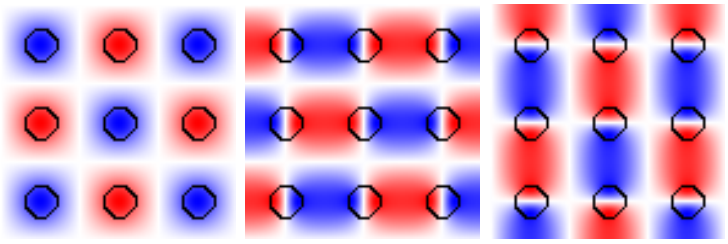

Figure 6.3: Electric field distribution for the first three bands of the TM modes of fig. 6.2 at k-point M. The second and third mode are degenerate. In each image, color indicates the amplitude of the field (either positive or negative) along the z axis and white means zero field.

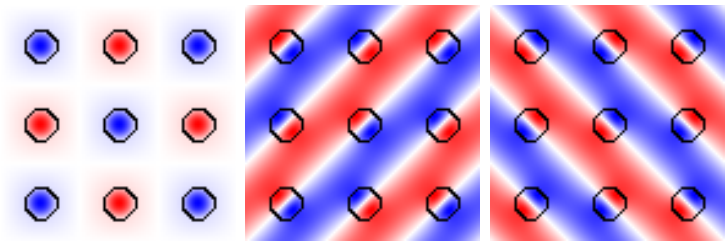

Figure 6.4: Magnetic field distribution for the first three bands of the TE modes of fig. 6.2 at k-point M. The second and third mode are degenerate.

so the matrix is made up of thin dielectric veins: the structure and the corresponding Brilloiun zone are depicted in figure 6.5.

As we did in the previous section, we show the dispersion curves both of TM and TE modes all over the high symmetry path delimiting the irreducible Brillouin zone.

In this case we can clearly see that there is a frequency region where neither TM nor TE modes exist, giving rise to a complete bandgap that extend itself all over the $\mathbf{k}_{\|}$ path in the irreducibile Brillouin zone.

Again we can visualize the electric and magnetic field distribution to see how the modes look like below and above the gap.

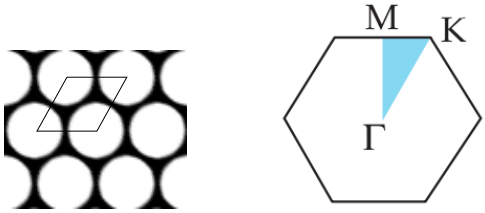

Figure 6.5: On the left, a cross-sectional view of the dielectric function of the 2D triangular photonic crystal; on the right, the corresponding 2D Brillouin Zone, with the irreducible zone highlighted and delimited by high symmetry points.

6.4 Surface States

Until now the discussion has concerned the interior of photonic crystals of infinite extent, not taking into account the fact that real crystals are necessarily bounded by surfaces. For a surface mode, light is localized at a surface plane and the field amplitudes decay exponentially away from the surface. They decay within the crystal because of the band gap, and they decay within the air region because they lie below the light line $\omega = ck_{\parallel}$.

We can characterize a given surface by its inclination and its termination. Surface inclination specifies the angles between the surface normal and the crystal axes. Surface termination specifies exactly where the surface cuts across the unit cell; for example, we can end a two-dimensional lattice of circles by stopping after some whole number of circles, or by cutting each circle in half at the boundary, or by cutting off some arbitrary fraction.

We will focus on the surface states of a square lattice of dielectric columns, but many of the arguments and results that we present can be extended to other cases and considered quite general. We will examine the same square array of alumina rods with $\varepsilon = 9.2$ that experimentally showed focusing properties.[34] Consider the TM band structure, which has a photonic band gap between the first and second bands. For our surface inclination, we choose planes of constant x, otherwise known as the (10) surface of the square lattice according to the Miller indices.[57]

This structure has continuous translational symmetry in the z direc-

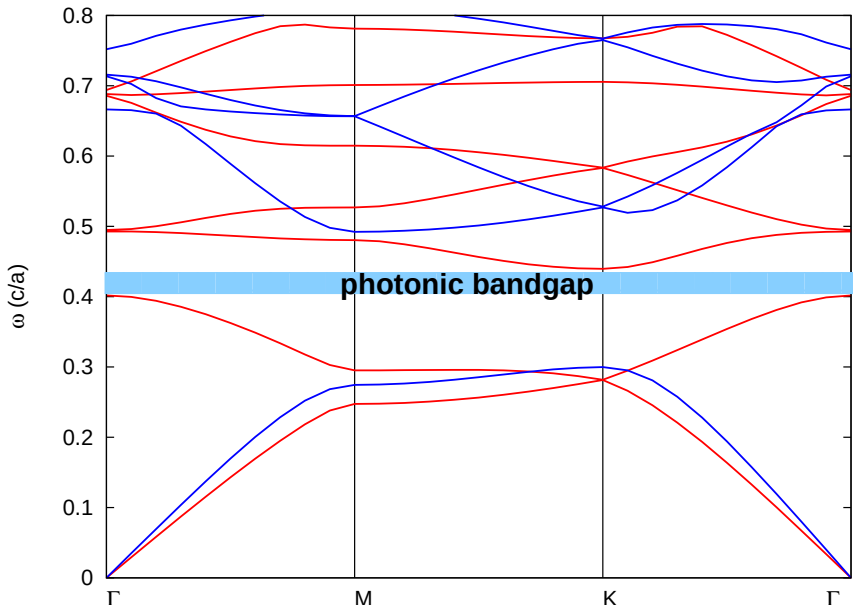

Figure 6.6: Photonic band structure for a 2D PC with air columns in a dielectric matrix. The matrix has dieletric constant of $\varepsilon = 12$ and the holes have radius $r = 0.45a$. Red bands are TM modes and blue bands are TE modes. Frequencies ω are expressed as dimensionless unit c/a and must be scaled to the corresponding lattice constant a to obtain experimental frequency in Hz. Both TM and TE mods present a photonic band gap in the same frequency region, highlighted. Calculation made with MPB.[64]

tion, so we can describe the modes by a k_z wave vector, but we restrict ourselves to $k_z = 0$. We have broken translational symmetry in the x direction but have maintained it in the y direction in the plane. Thus, k_y is conserved, but k_x is not conserved. Therefore, it is useful to compute the projected band structure of the infinite crystal, in which (k_y, ω) is plotted for each $\omega_n(k_x, k_y)$.

Figure 6.4 shows the projected band structure of the constant$-x$ surface of the square lattice of dielectric rods. In order to understand it, we first consider the projected band structures of the outside air and

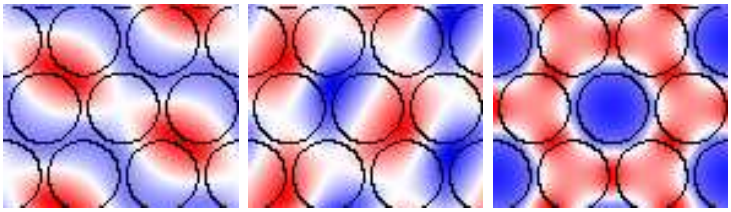

Figure 6.7: Electric field distribution for the first three bands of the TM modes of fig. 6.3 at k-point K. The first two modes are degenerate, and the third is just above the complete photonic band gap.

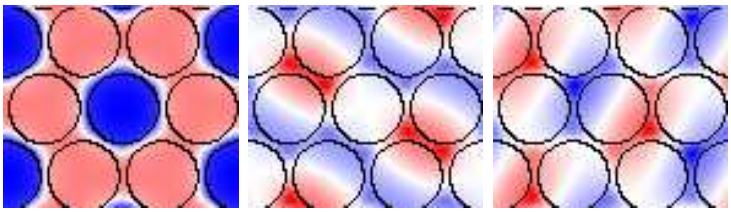

Figure 6.8: Magnetic field distribution for the first three bands of the TE modes of fig. 6.3 at k-point K. The second and third mode are degenerate.

the photonic crystal separately.

For a given k_y, there are light modes at all frequencies above the light line: these modes where $\omega \geq c|k_y|$ are the mode belonging to the light cone.

Along the light line $\omega = ck_y$, the light travels parallel to the surface, and increasing ω at fixed k_y corresponds to increasing k_x. The union of light cone with the photonic bands of the slab calculation (shaded in light blue) represents the projected band structure of the photonic crystal. Note that the photonic crystal contains a TM band gap.

Now we can distinguish among the three types of surface states of the projected surface Brillouin zone: light that is transmitted (slab photonic bands above the light cone), light that is internally reflected (slab photonic bands below the light cone), and light that is externally reflected (the region of the light cone where no photonic bands belonging to the slab exist). In the region of (ω, k_y) where the modes are extended in

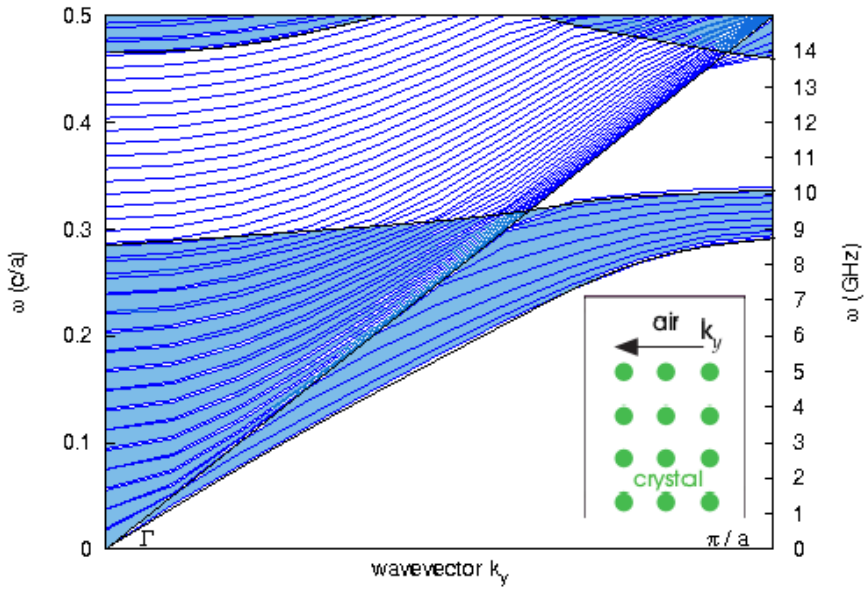

Figure 6.9: Projected band structure of the square lattice slab of alumina rods in air. Photonic bands belonging only to the slab are shaded in light blue. The crystal is terminated as shown in the inset; this type of termination doesn't support any surface state.

both the air and in the crystal, it is possible to transmit light with those parameters through the crystal. In the region where the modes are in the crystal, but they are beneath the light line of the air modes, the light can extend into the crystal, but decays exponentially into the surrounding air. This is nothing but the familiar phenomenon of total internal reflection. In the reflective region instead, the situation is reversed. There, the modes can extend into the air, but they decay exponentially into the crystal.

Finally, there might exist surface modes, which decay exponentially away from the surface in both directions, but the terminated square array doesn't support any of those modes. Such a mode appears if we introduce another type of defect, cutting in half the columns that belong

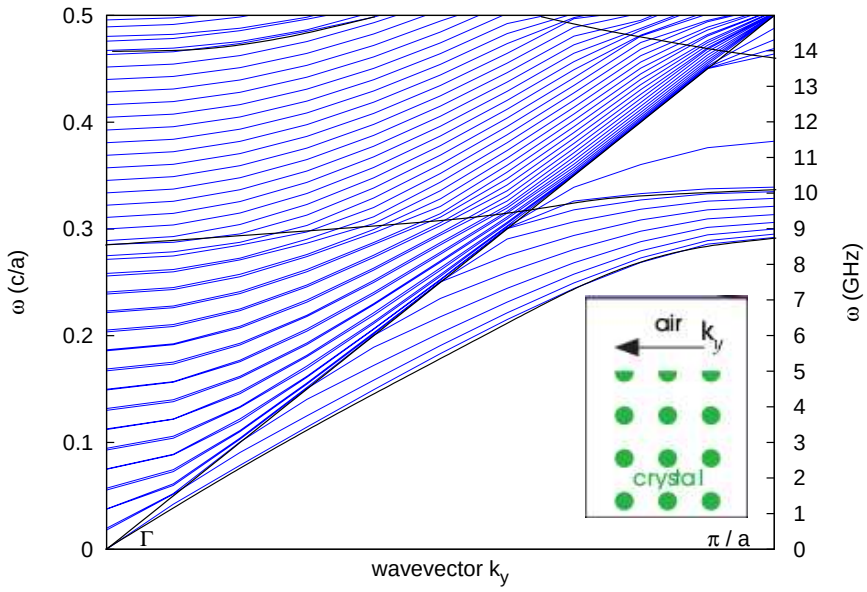

Figure 6.10: Projected band structure of the square lattice slab of alumina rod in air terminated with an array of columns cut in a half. This kind of termination gives rise to the surface mode clearly visible in the middle of the gap.

to the surface. Figure 6.4 shows the band structure of such a surface structure. The localized surface modes in the are below the light line of the air modes, and are also within the band gap of the crystal. The fields therefore decay exponentially in both directions, and the mode is pinned to the surface plane, as shown in figure 6.4. By exciting such modes, we can imprison light at the surface of the crystal.

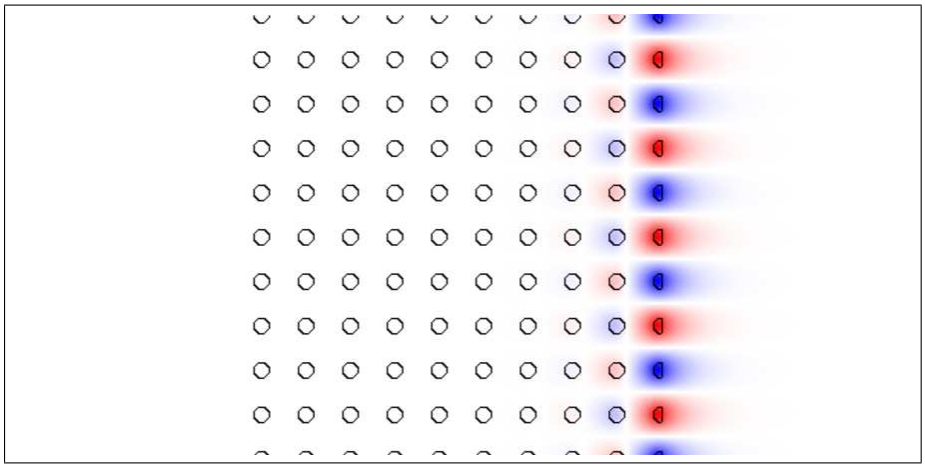

Figure 6.11: Electric field distribution in the z direction associated with a localized surface state, originated by truncating a square lattice of alumina rods in air, cutting each rod of one of the two surfaces delimiting the slab. The mode shown corresponds to a surface parallel wavevector of $k_y = \pi/a$. The calculation run to obtain this field pattern uses a separation between two periodic replica of the slab equivalent to 4 times the slab thickness, which is 10 layers of columns.

Chapter 7

Two-dimensional 12-fold Photonic Quasicrystal

We proceed now to study a two-dimensional photonic quasicrystal, in particular a 12-fold system obtained by Stampli inflation[79] and already examined by experimental techniques and calculations.[14,16] Alumina rods with dielectric constant $\varepsilon = 8.6$ and radius $r = 0.3a$ are placed at the vertices of this type of tiling which is made up of squares and equilateral triangles both with side a, as shown in figure.7.1

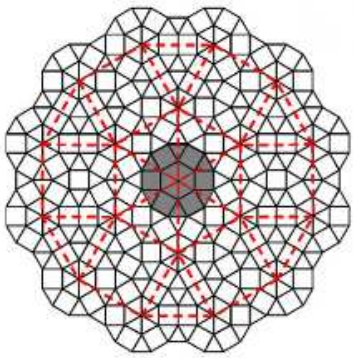

Figure 7.1: Illustration of the Stampfli inflation rule. Starting from the parent tiling represented by the gray-shaded central dodecagon, a big parent (red dashed lines) is generated by applying an inflation factor of $\sqrt{3}+2$ and filled up by copies of the original dodecagon placed at its vertices.

Previous investigations showed that a portion of this type of quasicrystal cut in shape of a wedge[14] or a slab[16] exhibits negative refraction and focusing properties at a particular frequency. It's still not precisely clear though what is the physics that gives rise to these phenomena, since further investigations[17] show a strong dependance on slab thickness, surface termination and position of the incident light beam.

With the calculation of dispersion curves and equifrequency surfaces

of this kind of systems we try to get an insight of its optical properties.

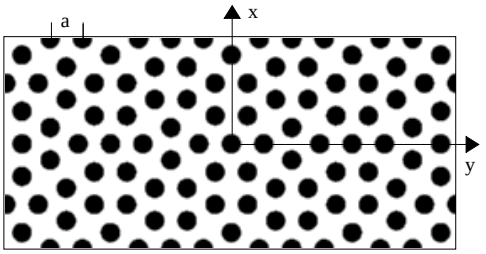

Figure 7.2: Dielectric distribution of the supercell approximant used for the calculations. The supercell consist of 116 columns of alumina with $\varepsilon = 8.6$, radius $r = 0.4$ and lattice constant $a = 1.33$. Periodic boundary conditions in x and y direction are imposed, introducing translational symmetry that doesn't belong to the concept of quasicrystal.

We don't want to perform simulations of a huge quasicrystalline system because it would be computationally demanding, so we restrict ourselves to a smaller portion cut from the 12-fold tiling and, due to the nature of the planewave code, we use it as a supercell and replicate it with boundary conditions on the two dimensions, as shown in figure 7.2. In this way we are introducing translational symmetry in our system, so strictly we shouldn't speak anymore of quasicrystals, but it has been reported that many properties of quasicrystals already show up in small constituent parts of the tiling.[13]

7.1 Single Slab: Results of the Calculations

The TM band structure calculation for the photonic bands of such a supercell is plotted in figure 7.3. This structure exhibits a complete band gap for this polarization over a wide frequency range, of the order of $0.1c/a$. We want to point out that the other polarization, i.e. the TE modes, doesn't have any band gap. We add a GigaHertz scale to give

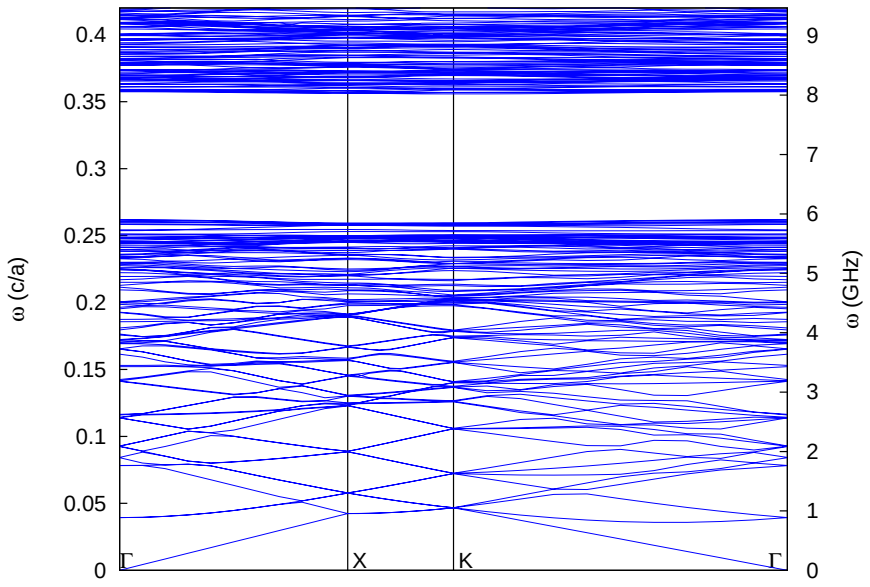

Figure 7.3: Photonic bands of TM modes for the 12-fold quasicrystal approximant of fig. 7.2. The main feature is the wide (in frequency) complete band gap. The bands grow thicker and thicker as the frequency rises also because of band folding. The GHz scale on the right corresponds to a system with lattice constant $a = 1.33$ cm. It should be noted that there is no gap for TE polarization in this system.

an idea of the frequency ranges for this system when we keep the same parameters used in previous investigations,[16,17] namely a cylinder radius $r = 0.4$ cm on a lattice constant $a = 1.33$ cm.

We performed additional calculations to see whether experimental deviations from the ideal conditions could affect the dispersion characteristics of the system. Deviations in the value of the source frequency used for experimental measurements can be ruled out since its precision can reach $10^{-6}c/a$. The two other sources of discrepancies to an ideal situation are a random error in the positioning of the cylinders, that are tipically displaced by an automated robot with an error of ± 0.1 mm,

and a deviation in the value of the dielectric constant declared by the manufacturer of the alumina cylinders, that can reach $\Delta\varepsilon = 0.1$.[80]

To introduce a random error on the cylinders' position we choose to move each element by a displacement (in both x and y coordinates) extracted from a gaussian distribution with $\sigma = 0.1$ mm. To check the effect of a deviation in the value of ε we recalculate the photonic bands changing its value to 8.5 and 8.7 in all the cylinders. In each of the aforementioned situations there is no evidence of changes in the dispersion characteristics of the systems, since the eigenfrequencies undergo a maximum shift of $10^{-4}c/a$.

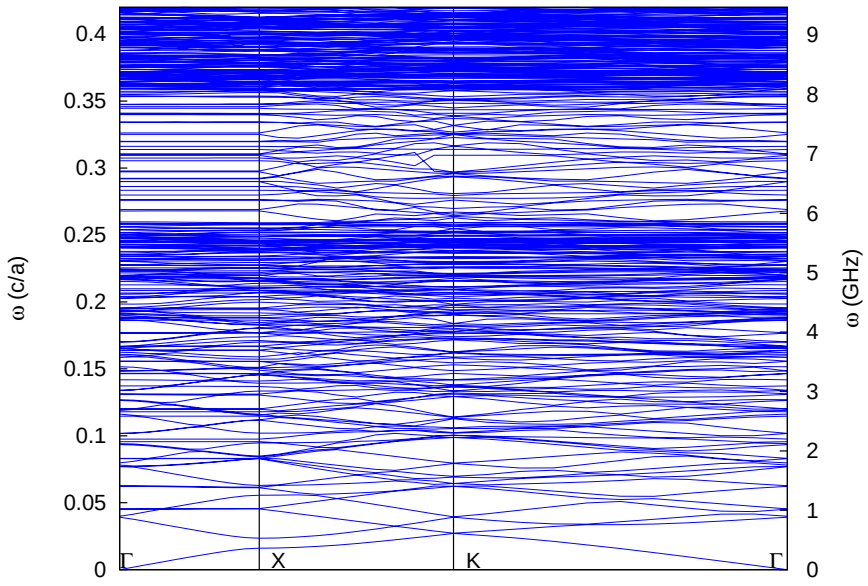

Figure 7.4: Photonic bands of TM modes for the 12-fold quasicrystalline slab. Breaking the translational symmetry with the insertion of the vacuum region completely fills up the photonic bandgap with defect states.

We now move to a calculation of a supercell that closely resemble the experimental setup where focusing occurs,[16] introducing a vacuum region in one direction to simulate the properties of a slab cut from a

bigger parent tiling. The new supercell consist of the same supercell depicted in figure 7.2 plus a vacuum region with twice the thickness of the slab, that separates two replica of the slab.

As expected, the presence of a vacuum region gives rise to a number of defect states that completely fill up the TM photonic bandagp as can be seen in figure 7.4. This time there is not an immediate way to distinguish among states propagating only in air, only in the photonic quasicrystal, in both of them or surface localized, due to the entanglement of the dispersion curves. The only way to look for the presence of surface modes is to examine the field distribution of the modes in the frequency range of the gap seen in the photonic bands of figure 7.3.

The analysis of filed patterns shows that there are no surface localized states, so that negative refraction and focusing cannot be traced back to the presence of such states. We thus try to give an interpretation of the optical properties in terms of negative group velocity and shape of the equifrequency surfaces (EFS).

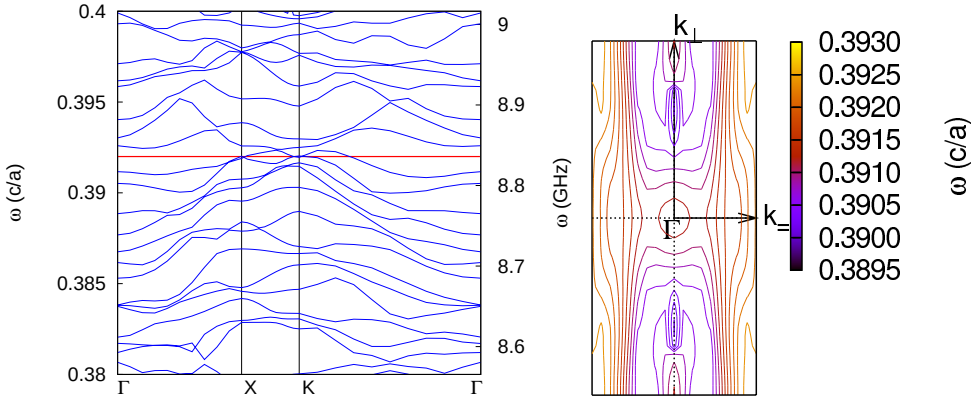

Figure 7.5: Magnification of the photonic bands of figure 7.4 around the frequency $\omega = 0.392c/a$, indicated by the red line. On the right, the EFS plot in the frequency range of interest.

We fix our attention to the frequency value that was used to obtain focusing in the first place,[14,16] that is $\omega = 0.392c/a$. If we look at the red

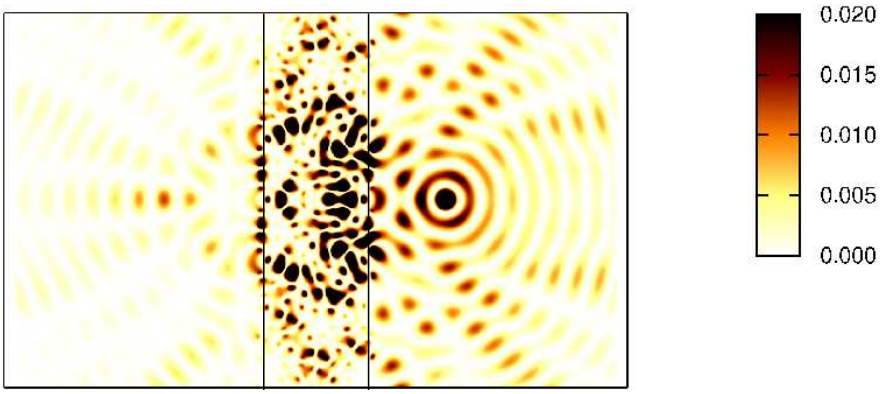

Figure 7.6: Simulated intensity field maps for a Gaussian pulse centered on frequency $\omega = 0.392c/a$ with normal incidence, directed to the center of the central dodecagon of the 12-fold quasicrystalline structure. The source is located at the right of the slab (big dark spot) at a distance that is a half of the slab thickness, the focus comes out on the opposite side. Intensity units are arbitrary.

line in figure 7.5 that crosses a magnified region of the dispersion curves, it seems indeed that the bands at that particular frequency have negative curvature and thus negative group velocity. The FDTD simulation in figure 7.6 of the system in those same conditions confirms once more the formation of a focus.

Further investigations[17,56] set the optimal frequency to get focusing to $\omega = 0.394c/a$: from the magnified dispersion diagram of Fig. 7.7 we can see that this frequency too crosses bands with negative curvature, again from the FDTD calculation (Fig. 7.8) we get a confirmation of the formation of a focused spot that is a bit more intense than the previous one.

Looking at another magnified region of the dispersion bands in Fig. 7.9, we choose another frequency where we find more bands with negative curvature, for example $\omega = 0.403c/a$: the corresponding FDTD simulation shows a more intense focus, as can be seen in figure 7.10 and

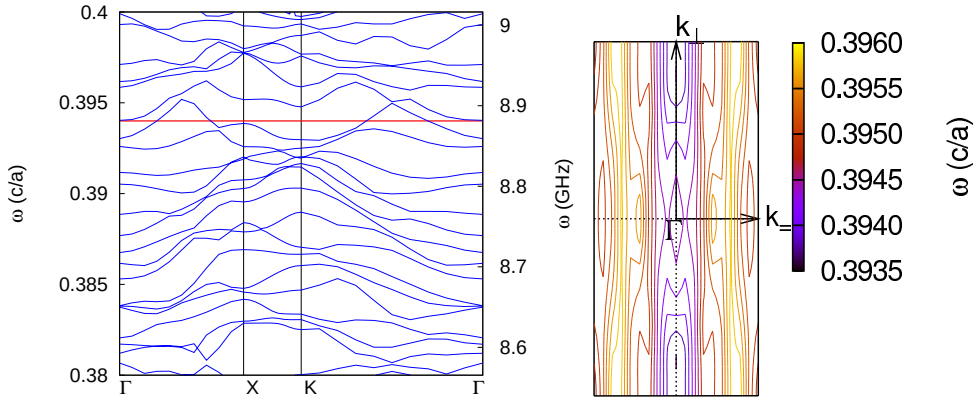

Figure 7.7: Magnification of the photonic bands of figure 7.4 around the frequency $\omega = 0.394c/a$, indicated by the red line. On the right, the EFS plot in the frequency range of interest.

in 7.11 where we do a comparison among the spot intensities of the three cases studied above.

The lack of experimental measurements at the higher frequencies we are examining prevents a further confirmation of the predictivity of our approach. Still, we can rely with a good degree of confidence on the FDTD simulations since they are considered a robust technique.

The use of dispersion bands and EFS to predict focusing are tools that must be used with care though, because in some frequency regions that apparently look favorable to obtain focusing, such as $\omega = 0.407c/a$ in figure 7.12, the focus almost disappears in the FDTD simulation of figure 7.13. This is probably due to contributions coming from some parts of the photonic bands where the curvature is positive, something that it's hard to discern when the band structure has so many neighbouring states.

In conclusion, wa saw that the analysis of dispersion curves and equifrequency surfaces can give an insight into the focusing properties even of an object with the degree of complexity of a quasicrystal. Due to the lack of translational symmetry in quasicrystalline systems and

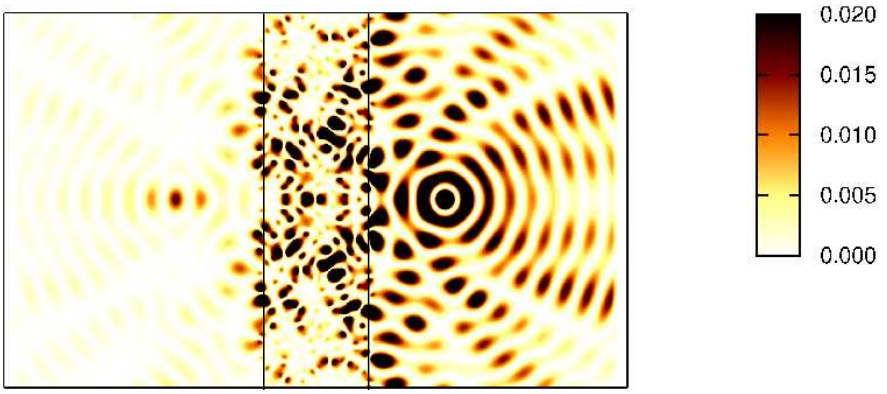

Figure 7.8: As in figure 7.6, but for $\omega = 0.394c/a$.

the consequent necessity to use an approximant and thus a supercell approach, both the dispersion curves and the EFS are characterized with a great density of data.

Obtaining precise information from these entangled data is not straightforward, so we suggest to use these computational tools with some care, especially for the supelensing and focusing properties. We will see in the following sections that there are other properties of quasicrystalline slabs besides superlensing and focusing that can be explored with the methods used here.

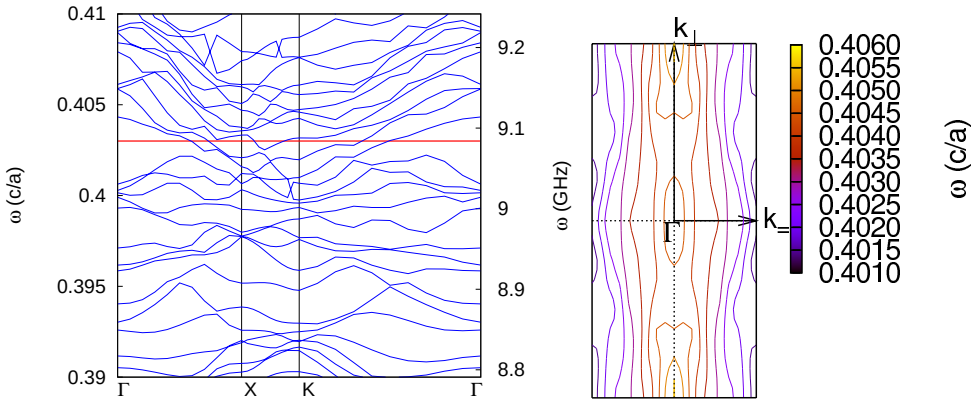

Figure 7.9: Magnification of the photonic bands of figure 7.4 around the frequency $\omega = 0.403c/a$, indicated by the red line. On the right, the EFS plot in the frequency range of interest.

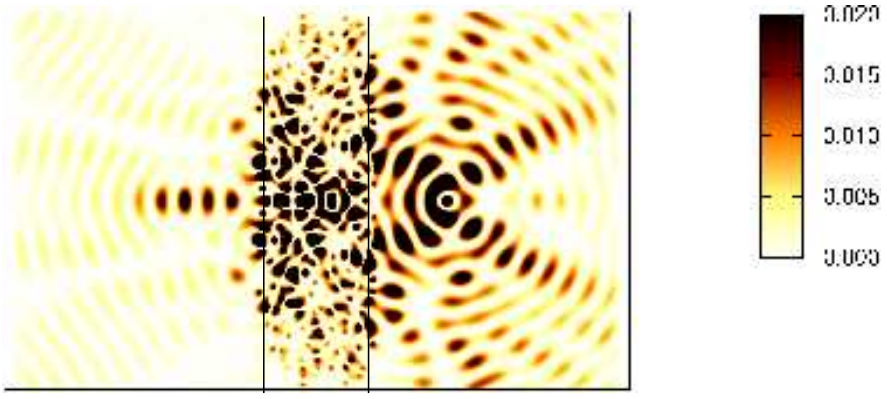

Figure 7.10: As in figure 7.6, but for $\omega = 0.403c/a$.

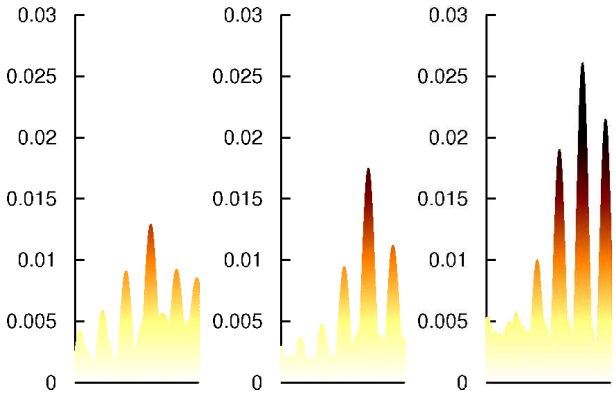

Figure 7.11: Spot intensities for the focusing at $\omega = 0.392$, 0.394 and 0.403 respectively. Intensity units are arbitrary but on the same scale.

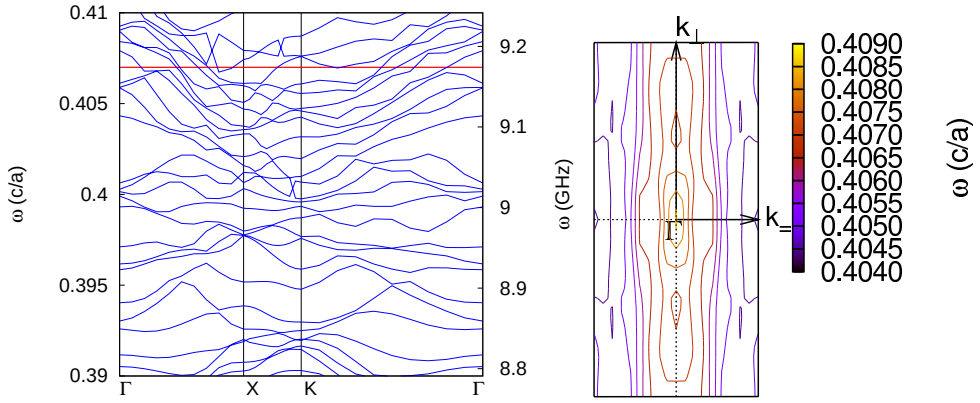

Figure 7.12: Magnification of the photonic bands of figure 7.4 around the frequency $\omega = 0.407c/a$, indicated by the red line. On the right, the EFS plot in the frequency range of interest.

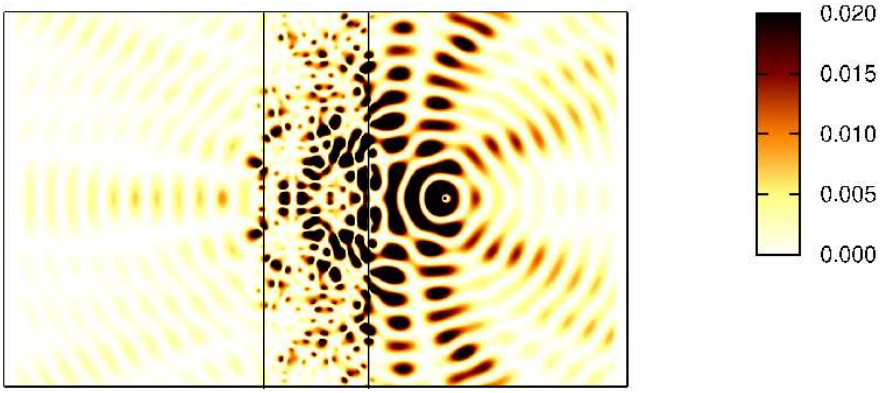

Figure 7.13: As in figure 7.6, but for $\omega = 0.407c/a$. At this frequency, focusing intensity is negligible.

7.2 Special solutions for the Single Slab and Microcloaking

Since the dispersion curves for this 12-fold quasicrystalline single slab are too dense and entangled, the only way to determine whether this system supports localized modes in the surface region is to look through all the images that show the electric field distribution.

As we pointed out in Section 7.1, we found no such localized states in the slab, but the modes we examined from the electric field distribution show interesting features nonetheless.

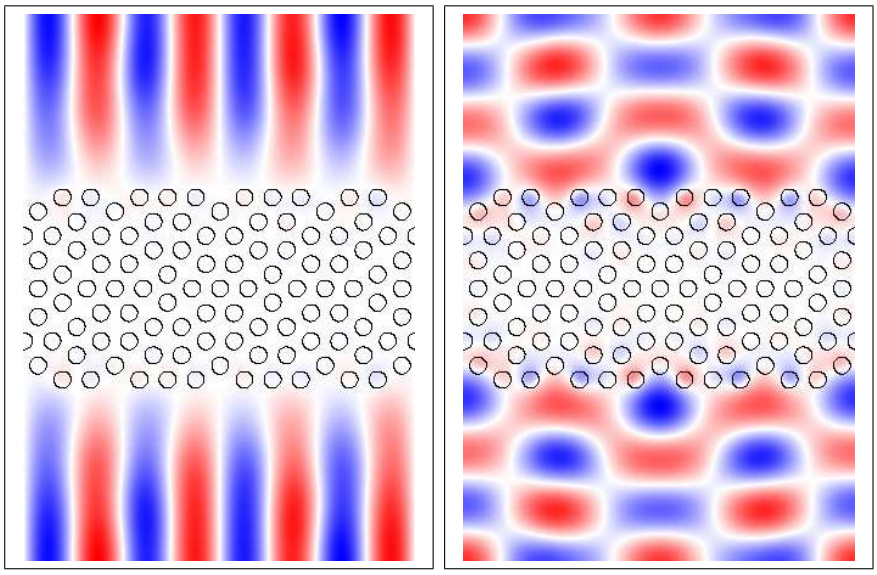

Figure 7.14: Electric field patterns of two modes at k-point Γ with frequencies 0.290 and 0.305 c/a, respectively. It's evident from the field distribution that they propagate only in the vacuum region, decaying into the slab.

In the frequency range $0.26 - 0.35$ c/a, where the 12-fold quasicrystal exhibits a complete photonic band gap (see Fig. 7.3), there exists no modes. When we introduce the vacuum region, thus creating a slab, the gap becomes completely filled with defect modes. Examining the

electric field patterns, those modes predictably propagate only in the vacuum region, looking like the ones shown in Fig. 7.14.

In such a complex system as this 12-fold quasicrystalline slab, field patterns become increasingly weird and unpredictable with increasing frequencies. While the search for surface localized modes is unsuccessful, browsing all the possible field distributions gives us a hint to exploit this kind of photonic quasicrystal for other purposes than superlensing.

In the field of metamaterials and their applications to electromagnetic waves, the realization of the cloak in the microwave frequencies[1] is surely one of the most fascinating examples.

In Section 7.1 we saw that incident electromagnetic radiation from a source may give rise to a focus on the other side of the slab. In the frequency range useful for focusing, the EM radiation propagates through the whole slab, as can be seen in the FDTD simulations shown in Fig. 7.6 and following.

In a frequency range above the gap we found several modes that live in air and only in some regions of the quasicrystalline slab, excluding one or more dielectric cylinders from the propagation of EM waves, as illustrated in Fig. 7.15.

In analogy to the microwave cloak case, we can imagine the quasicrystalline structure of the slab as a cloak operating at a precise frequency, hiding determined areas of the slab itself from EM waves.

What we suggest as a possible application is to use the slab presented here as a strip containing data, stored or embedded in some way within the slab, that can be read with EM waves at a fixed frequency. If we want to prevent some data from being read, they can be located in the cloaked area at that particular frequency; these hidden data would then need EM waves at a different frequency to be accessed.

Maybe the quasicrystalline slab presented here doesn't seem to be a proper invisibility cloak, since is not engineered with the purpose of steering EM waves around an object.

We would like to point out though that this kind of quasicrystalline

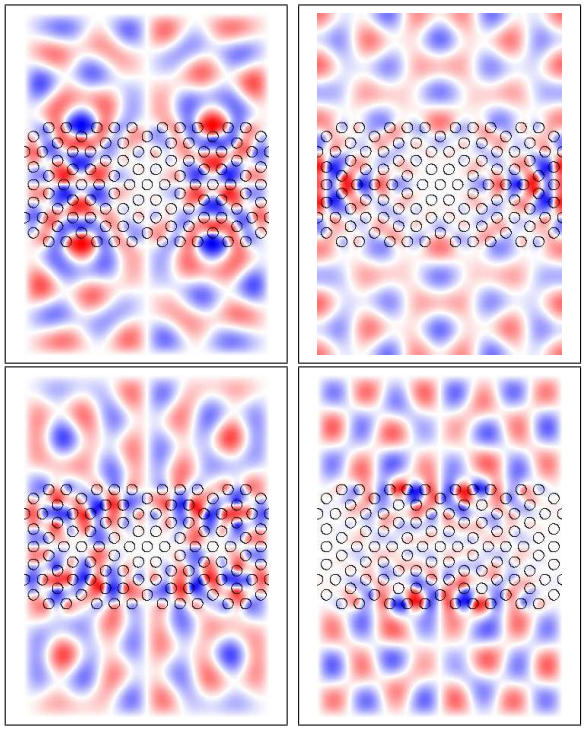

Figure 7.15: Electric field patterns of four modes at k-point Γ with frequencies 0.355, 0.362, 0.367 and 0.376 c/a, respectively. These modes propagate outside the slab and inside the slab they live only in some areas, excluding one or more cylinders from EM waves.

structure, compared to a periodic crystalline material, is characterized by a large amount of intrinsic defects that are able to guide waves in a nontrivial way, achieving the same aim of a cloak, hiding an area of space from the propagation of those very waves.

This example suggested us to investigate if the peculiar properties of systems based on quasicrystals could be further explored in other configurations, and a different and interesting physical property will be discussed in the following section.

7.3 Double Slab and Photon Localization

Besides superlenses, other devices based on 12-fold quasicrystals have been studied, such as antennas[18] or resonant cavities,[15] so we move on to investigate another possible configuration based on the same 12-fold slab.

We choose to examine the behaviour of a system made up of two 12-fold quasicrystalline slabs seen before, separated by a vacuum layer thick a half the thickness of one slab, as depicted in figure 7.16. We therefore calculate the TM photonic bands for this system, using as usual a supercell with the slab and a vacuum region.

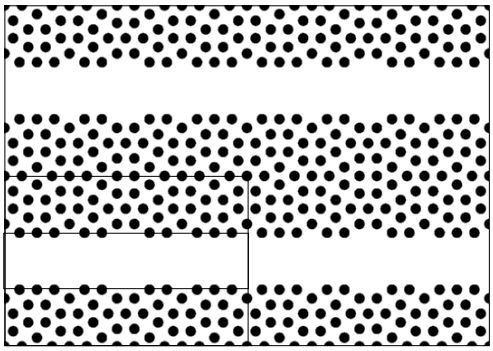

Figure 7.16: Dielectric function of the supercell used for the calculation, replicated twice in both dimensions. A single supercell is highlighted, which is divided in three parts to show that the thickness of the vacuum region is exactly half the thickness of the slab.

The dispersion curves of Fig. 7.17 show some interesting features. The smaller vacuum layer leads to only a few defect states in the frequency range of the photonic band gap, but we want to point out the presence of a particular band just below $\omega = 0.3c/a$ that is completely flat, and thus dispersionless, over the whole brillouin zone.

No dispersion suggests a very strong localization of such a mode, so we proceed to check its behaviour looking at the electric field distribution within the structure.

Figure 7.18 shows indeed a strongly localized field pattern in the vacuum region between two slabs. The mode appears like a dipole confined between two indentations of the slab surface. In particular, the mode lives only in proximity of those indentations made up of four cylinders,

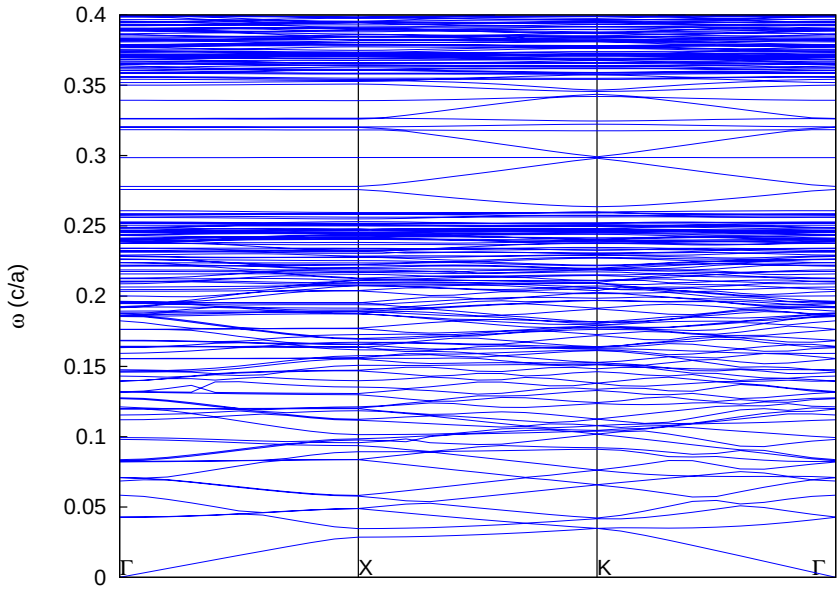

Figure 7.17: TM photonic bands for the supercell seen in figure 7.16, where the nearest replica of the slab is separated by a vacuum region with a thickness that is the half of the slab's thickness. A few defect modes in the frequency range of the gap are distinguishable and a single flat mode can be seen just below $\omega = 0.3c/a$ (the calculation gives $\omega = 0.298519c/a$ at Γ and $\omega = 0.298615c/a$ at K and X).

that are a kind of intrinsic surface defects that come out naturally once the surface itself is created from a quasiperiodic system.

The presence of intrinsic defects is a key feature of quasicrystals which can be exploited to study new properties and phenomena. In periodic photonic crystal these would show up only in presence of engineered defect that must be created and tuned on purpose, because they don't belong to the original lattice.

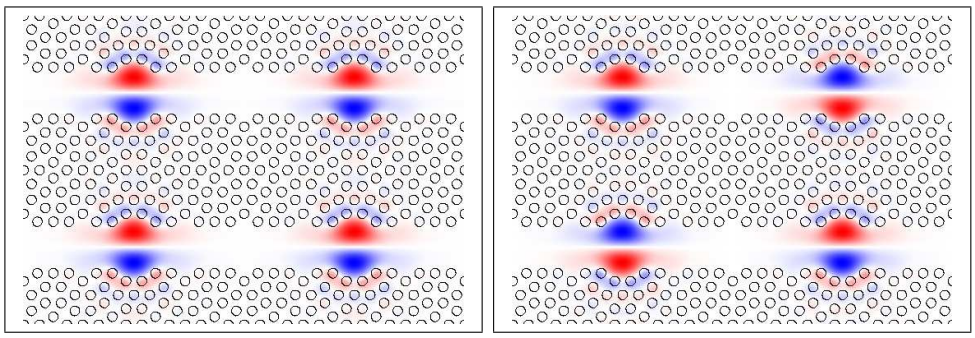

Figure 7.18: Electric field pattern for the localized mode at $\omega = 0.299c/a$ seen in figure 7.17, visualized at $k-$points Γ and K (center and corner of the Brillouin zone, respectively). The mode is clearly localized in the vacuum region between two slabs in proximity of an indentation of the slab surface that rises naturally from the creation of the surface itself. The field distribution in different $k-$points is exactly the same, with only a difference in phase between neighbouring replicas when $k_{\|} \neq 0$.

7.4 Characterization of the Localized Photonic Mode

The next step is to see whether this localized mode survives at different slab separations (i.e. different thickness of the vacuum layer). We thus add a little more of vacuum, first a layer with $a/2$ and then with a, and recalculate the photonic bands to see if the dispersion of this mode is affected.

Looking at figure 7.19 it becomes evident that the dispersion of the localized mode is affected even by a small change in the thickness of the vacuum region.

When we add a vacuum layer of $a/2$ (left panel) the localized mode lowers its frequency ($\omega = 0.276c/a$) and if we add another $a/2$ it disappears from the dispersion bands (right panel), going below the gap frequency range and mixing with the continuum of the photonic bands.

If we instead reduce the vacuum region between the two slabs, we

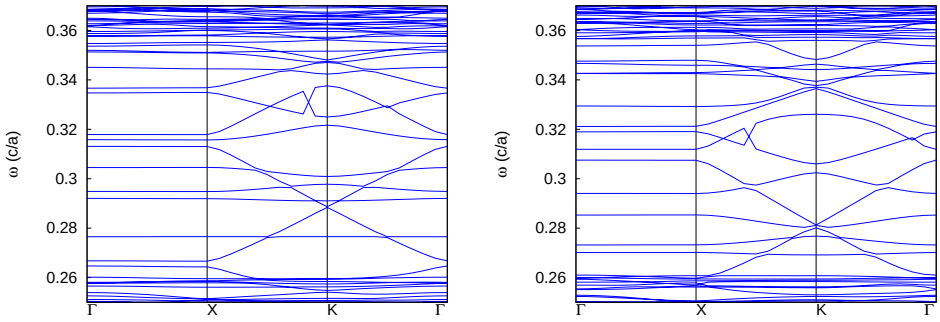

Figure 7.19: TM photonic bands for a supercell similar to the previous one, where the vacuum region separating to slabs is expanded by half a lattice constant a (left panel) and a whole a (right panel). The dispersion curves are magnified in the frequency range of the photonic gap. The localized mode shifts to a lower frequency of about $\omega = 0.276c/a$ in the first case, and disappears in the latter.

obtain the opposite effect: the localized mode is pushed towards higher frequencies. In figure 7.20 we plot the frequency dependence of the localized mode on the vacuum layer thickness: it appears that the frequency decreases linearly when increasing the distance between two slabs.

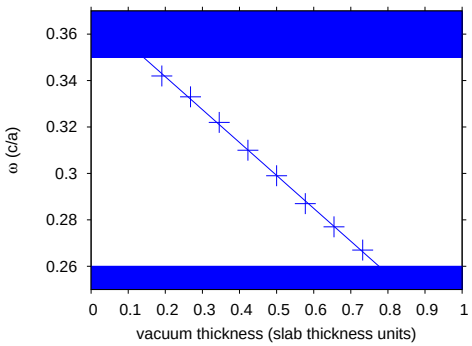

Figure 7.20: Frequency dependence of the dispersionless localized mode on the distance between the two slabs. The vacuum layer thickness is expressed as a function of the slab thickness. The mode frequency decreases linearly with increasing vacuum layer thickness. Blue shaded areas are the band continuum below and above the photonic bandgap.

7.5 Excitation of the Localized Photonic Mode

In this case FDTD simulations should give us an insight of how such a localized photonic mode can be excited. We then perform a calculation where a gaussian pulse centered precisely at the frequency of the localized mode is normally incident to the slab and observe the time evolution of the system.

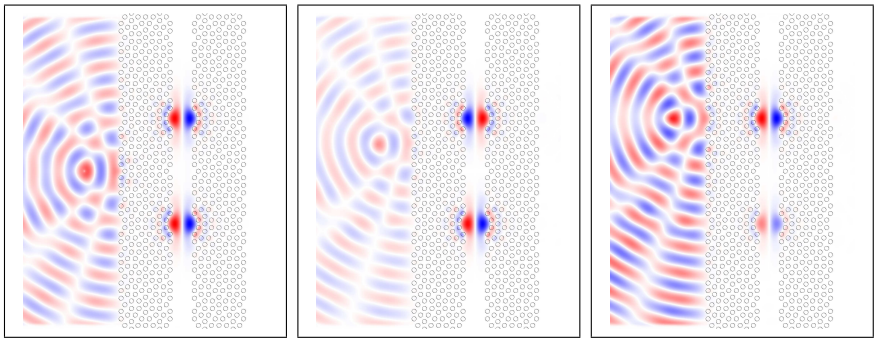

Figure 7.21: Snapshots of the time evolution of a gaussian pulse centered on frequency $\omega = 0.299c/a$ normally incident on the surface of the quasicrystalline slab. The source is located at the left of the two slabs, each time at the same distance from the surface but with a different lateral position: the localized photonic mode appears excited every time in two different but geometrically equivalent indentations of the surface.

As can be seen in figure 7.21 the localized mode can indeed be excited and its excitation doesn't seem to be related to the position of the source with respect to the local geometry of the quasicrystalline slab, in opposition to what happens in the case of superlensing.[17]

We perform FDTD simulations changing the lateral positions of the gaussian pulse: we start putting the source in front of the center of the 12-fold symmetry of the quasicrystalline geometry, then we move it in two steps towards the indentation of the slab surface where the localization takes place.

Apart from differences in relative field intensity and phase, the photons are localized in two geometrically equivalent positions, that are the same defective areas of the slab surfaces we identified in the field distribution of Fig. 7.18 obtained with the planewave calculation.

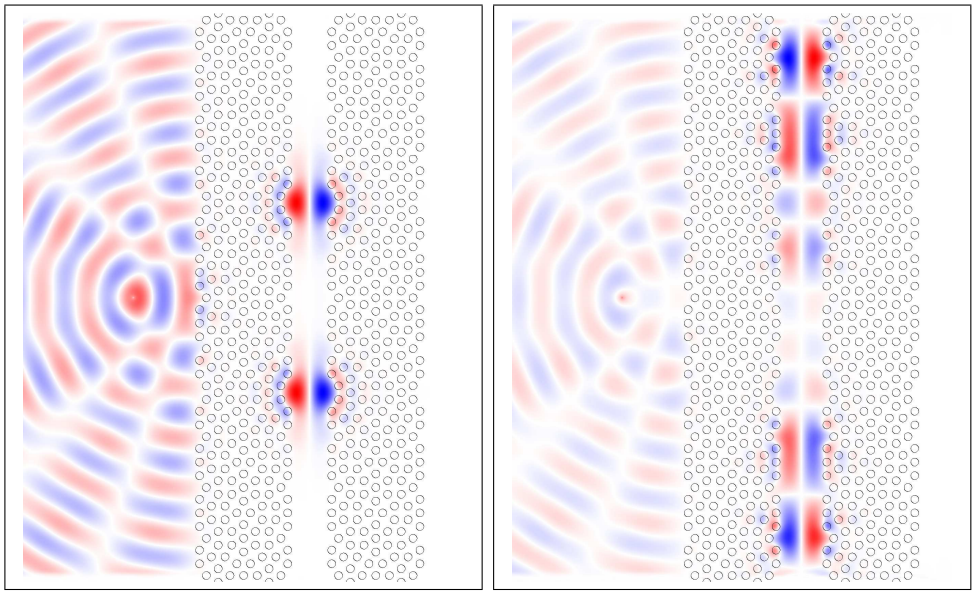

Figure 7.22: Snapshots of the time evolution of the same gaussian pulse centered on frequency $\omega = 0.299c/a$ as before, but with the source always in the same position and distance, while in the right image the vacuum layer between two slabs is thicker by $a/2$. The excited modes are propagating in the vacuum region, since the localized mode lowered its frequency.

If we stick to the same incident frequency but insert again an additional vacuum layer of $a/2$, we are no more exciting the localized mode because it shifts to a lower frequency, following the linear dependence we found out in Fig. 7.20.

We are instead exciting modes that propagate in the vacuum region, as shown in figure 7.22, where we compare the response of the two slabs at the same distance of Fig. 7.21 with those where we inserted a vacuum layer $a/2$ thick.

A further confirmation of the effective localization of photons in the system we are studying can be given examining snapshots of its time evolution in presence of a gaussian source.

We keep in mind (Section 5.5) that in the FDTD simulation we put perfect matching layers at the boundaries of the simulation cell. This boundary condition is chosen to avoid reflections and mimic open boundaries, thus absorbing the electromagnetic waves that comes in contact with the PML layer.

If we observe the sequence of snapshots in Fig. 7.23, all taken keeping the same arbitrary field intensity scale, we clearly see that the intensity of localized photon does not fade with time. Once the localized photonic mode has been excited by the incoming gaussian pulse, it continues oscillating with time without any attenuation.

The lack of intensity attenuation of the localized photon can be further confirmed by a comparison with the time evolution of the propagating modes of Fig. 7.24. In this sequence of snapshots we let evolve the photonic modes excited by the usual gaussian pulse centered at $\omega = 0.299c/a$ when the two slabs are separated by a further $a/2$ with respect to the previous case.

We use the same time scale of the series of snapshots of Fig. 7.23 and we can clearly see that in half of the time the field intensity has already faded considerably.

To be sure that perfect matching layers do act as open boundary conditions we perform a FDTD simulation inserting an additional layer of free space at the sides of the double slab, and we excite the propagating modes in the cavity, just like we did in the simulation of Fig. 7.24.

We can see in Fig. 7.25 that after the gaussian source has faded, the propagating modes become excited in the vacuum region and they radiate out of the cavity from the open side into free space, with fading intensity.

This just confirms that if we excite propagating modes between the two slabs, they will continue propagating with the vacuum layer acting

as a waveguide, and they will eventually radiate out of its open end.

If we instead excite a localized mode, there is no chance for the electromagnetic radiation to propagate in the vacuum waveguide, since photons will be stuck between the defective indentations of the surfaces.

The different behaviour of the system for localized and propagating modes suggests thus a possible use as a two state device, i.e. a switch.

As an example, this peculiar feature of the double quasicrystalline photonic slab could be exploited to build devices that can couple a mechanical (or vibrational, depending on the dimensions of the device) displacement that varies the distance between the two slabs with an incident TM polarized electromagnetic wave, acting as an optomechanical switch.

Here, the coupling takes place when the displacement acting on the relative positions of the two slabs causes either the localization or propagation of photons.

Recently, optomechanical coupling has been reported[81] in devices based on photonic crystals, which instead rely on radiation force exerted by band-edge modes that induces resonant vibrational modes in the system. This kind of coupling is reversed with respect to the effect we are proposing, but shows the current interest in how interaction between light and matter can be exploited using photonic crystals (or quasicrystals, in our case).

7.6 Point Defects and Cloaking

We now investigate also the double slab system for cloaking properties, as we did previously for the single slab in Section 7.2.

We focus our attention to possible effects on the photon localization due to defects in the quasicrystalline structure. If we want to hide some information, we can store it in a cylinder of the slab, and it could be that this information may alter the dielectric constant of the same cylinder. We could also think to use the defective cylinder itself to code

some information. In both cases it is crucial to see whether the photon localization is kept or destroyed by the presence of such a defect.

We perform two FDTD simulations with the same configuration for source frequency and vacuum separation of the central image of Fig. 7.21, only taking the alumina cylinder located at the center of the 12-fold rotational symmetry, first replacing it with a cylinder with $\varepsilon = 20.0$ and then removing it from the structure.

We show in Fig. 7.26 the results of these simulations. From the comparison among the three different cases it becomes evident that the presence of a point defect does not affect in any way photon localization, since the field distribution pattern is exactly the same, independently of the dielectric material seen by the incoming electromagnetic radiation. Field patterns not only look identical, they have also the same intensity since they are all plotted with the same color scale.

We can therefore conclude that the double quasicrystalline slab can hide objects and act as a cloak also when photon localization occurs. These combined effects surely suggest interesting perspectives for possible implementation in photonic devices.

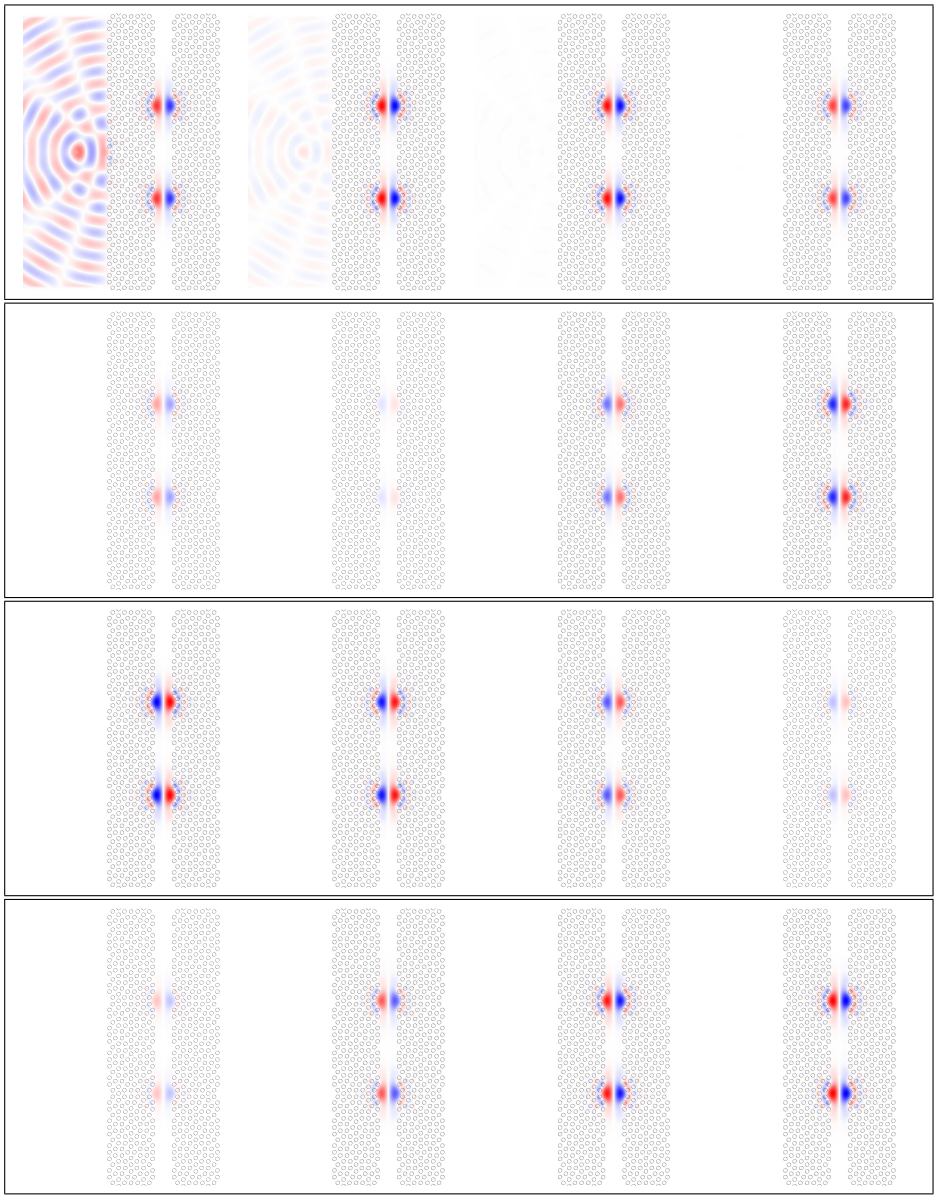

Figure 7.23: Snapshots of the time evolution of the same gaussian pulse centered on frequency $\omega = 0.299c/a$ as before, taken every 4000 timesteps (2.218 ns) of the simulation run. The two slabs are separated by a vacuum layer thick a half of the slab thickness. All the images have the same field intensity scale. This set of snapshots starts at a point where the gaussian pulse is fading and the localization of the photon is starting. The subsequent snapshots show the oscillation of the localized photonic mode without any attenuation of intensity. The evolution appears to be over one period but actually the localized mode oscillates over 200 times in the lapse shown here.

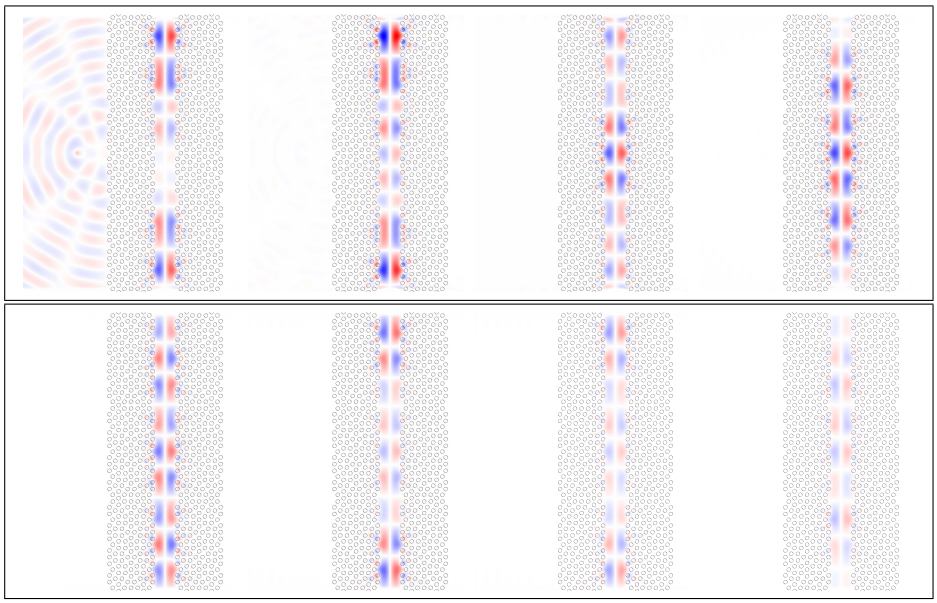

Figure 7.24: Snapshots of the time evolution of the same gaussian pulse centered on frequency $\omega = 0.299c/a$ as before, taken at every 4000 timesteps (2.218 ns) of the simulation run. The two slabs are separated by a vacuum layer thick a half of the slab thickness plus $a/2$. All the images have the same field intensity scale. This set of snapshots starts at a point where the gaussian pulse is fading and the photon starts propagating in the vacuum region. The subsequent snapshots show the oscillation of the photonic modes with consequent decaying of field intensity due to absorption from the perfect matching layers at the boundaries of the simulation cell.

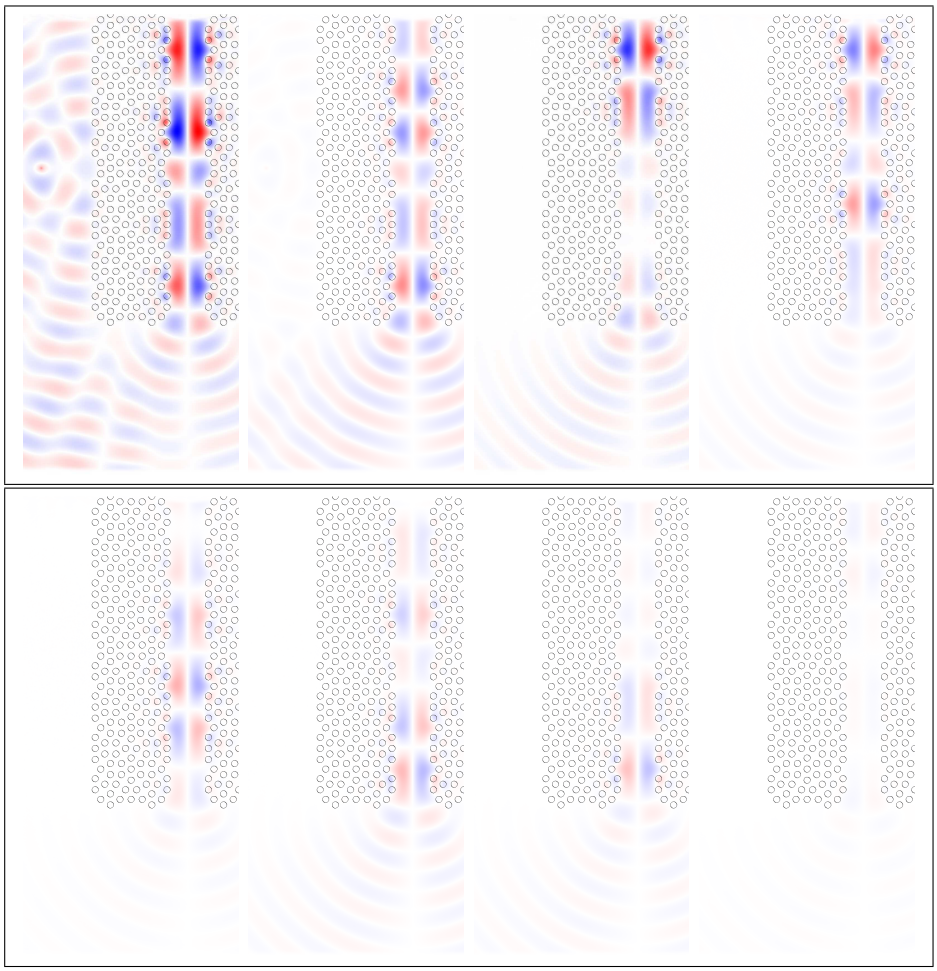

Figure 7.25: Snapshots of the time evolution of the very same system of Fig. 7.24 where we put some additional free space on one side of the double slab. The images are insets located near the boundary of the simulation cell and they all have the same field intensity scale. This set of snapshots starts at a point where the gaussian pulse is fading and the photon starts propagating in the vacuum region. The subsequent snapshots show electromagnetic waves coming out from the spacing between the two slabs, in addition to the oscillation of the photonic modes in the cavity and the consequent decaying of intensity.

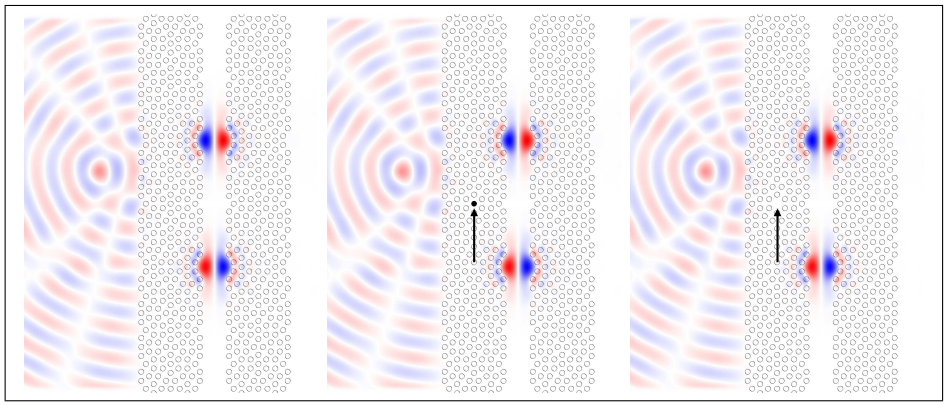

Figure 7.26: Presence of a point defect does not have any effect on photon localization. In the first image all the cylinders have the same dielectric constant $\varepsilon = 8.6$, in the second image the cylinder located at the center of the 12-fold rotational symmetry (in black) is replaced with one with $\varepsilon = 20.0$, and in the last image is removed. Snapshots are taken at the same instant during the time evolution of the system and with the same field intensity scale. The electric field distribution of the localized mode is exactly the same in any of the three cases, with or without the point defect.

7.7 Conclusions and Further Work

So far, we verified that metamaterials based on photonic quasicrystals can have superlensing properties and that the same type of material, in a different configuration, is able to localize photons and thus suggests the possibility to build new photonic devices, namely optomechanical switches.

We saw that a slab cut from a two dimensional 12-fold quasicrystalline tiling constitutes a metamaterial because of its effective refactive index that becomes negative in some frequency ranges. These regions of the spectrum where negative refraction and superlensing occurr can be found with the help of computational methods that calculate dispersion curves, equifrequency surfaces and electromagnetic field distribution of the system under study. In the particular case of quasicrystals, where the lack of translational symmetry forces to use big supercells, the amount of data and information contained in the dispersion curves and equifrequency surfaces is very dense and sometimes difficult to disentangle, suggesting particular care when predicting the behaviour of the physical system without the experimental counterpart.

Examiming the electromagnetic field patterns of the quasicrystalline slab we found that several modes could be useful for cloaking, since they do not propagate in the whole structure but they are inhibited to go through certain regions, that remain hidden at particular frequencies.

We think that other configurations of this kind of metamaterial give rise to interesting physical properties, more easily predictable, that can lead to the realization of new photonic devices. If we place two 12-fold quasicrystalline slabs together, separated by a vacuum layer of a precise thickness, we obtain the right conditions to localize photons between the two slabs. The localization takes place between two indentations of the slabs' surfaces, that are a kind of intrinsic defects formed when the surface are created from the bigger quasicrystalline lattice. This type of defects is unique to quasicrystalline systems and originates from their

lack of translational periodicity. The capability of localizing photons opens up the possibility of building devices exploiting this feature: for instance, we could realize a photonic switch with two states, one where the photon is localized and the other where the photon propagates, and as we discussed, the choice between these two states can be made only varying the distance between the two slabs.

This double slab system seems to be exploitable for cloaking too, since we saw that point defects in the lattice, characterized by a different dielectric constant, do not affect the localization properties of the device.

As a further work many of the results shown in this thesis should be experimentally verified even if we are confident that FDTD simulation gave a reliable confirmation. Furthermore, the realization of devices based on the localization of photons should be made with a practical application in mind, and therefore different dielectric materials could be explored.

Bibliography

[1] D. Schurig, J. J. Mock, B. J. Justice, S. A. Cummer, J. B. Pendry, A. F. Starr, and D. R. Smith, Science **314**, 977 (2006).

[2] J. D. Joannopoulos, S. G. Johnson, R. D. Meade, and J. N. Winn, *Photonic Crystals: Molding the Flow of Light - Second Edition* (Princeton University Press, Princeton, 2008).

[3] P. W. Anderson, Phys. Rev. **109**, 1492 (1952).

[4] S. John, Phys. Rev. Lett. **58**, 2486 (1987).

[5] J. P. Vigneron, J. F. Colomer, N. Vigneron, and V. Lousse, Phys. Rev. E **72**, 061904 (2005).

[6] J. P. Vigneron, J. F. Colomer, M. Rassart, A. L. Ingram, and V. Lousse, Phys. Rev. E **73**, 021914 (2006).

[7] M. Rassart, P. Simonis, A. Bay, O. Deparis, and J. P. Vigneron, Phys. Rev. E **80**, 031910 (2009).

[8] J. Aizpurua and J. P. Vigneron, in *Bio-Inspired Photonic Structures: Photonic Science and Engineering in the Living and Artificial Worlds*, Donostia International Physics Center (Abstract Book Editions, Donostia - San Sebastián, 2009).

[9] D. Shechtman, I. Blech, D. Gratias, and J. W. Cahn, Phys. Rev. Lett. **53**, 1951 (1984).

[10] D. Levine and P. J. Steinhardt, Phys. Rev. Lett. **53**, 2477 (1984).

[11] C. Janot, *Quasicrystals: A Primer* (Clarendon Press, Oxford, 1994).

[12] M. E. Zoorob, M. D. B. Chartton, G. J. Parker, J. J. Baumberg, and M. C. Nettl, Nature **404**, 740 (2000).

[13] H. Zhao, R. P. Zaccaria, J. F. Song, S. Kawata, and H. B. Sun, Phys. Rev. B **79**, 115118 (2009).

[14] Z. F. Feng, X. D. Zhang, Y. Q. Wang, Z. Y. Li, B. Y. Cheng, and D. Z. Shang, Phys. Rev. Lett. **94**, 247402 (2005).

[15] M. R. Masullo, A. Andreone, E. Di Gennaro, S. Albanese, F. Francomacaro, M. Panniello, V. G. Vaccaro, and G. Lamura, Microwave and Optical Technology Letters **48**, 2486 (2006).

[16] E. Di Gennaro, C. Miletto, S. Savo, A. Andreone, D. Morello, V. Galdi, G. Castaldi, and V. Pierro, Phys. Rev. B **77**, 193104 (2008).

[17] E. Di Gennaro, D. Morello, C. Miletto, S. Savo, A. Andreone, G. Castaldi, V. Galdi, and V. Pierro, Photonics and Nanostructures **6**, 60 (2008).

[18] A. Micco, A. Della Villa, V. Galdi, F. Capolino, V. Pierro, S. Enoch, and G. Tayeb, Phys. Rev. B **79**, 075110 (2009).

[19] J. Pendry, Phys. Rev. Lett. **85**, 3966 (2000).

[20] J. Pendry, Science **305**, 788 (2005).

[21] J. Pendry and D. R. Smith, Phys. Today **57**, 37 (2004).

[22] V. M. Agranovich and V. L. Ginzburg, *Spatial Dispersion in Crystal Optics and the Theory of Excitons* (Wiley, London, 1966).

[23] V. G. Veselago, Sov. Phys. Usp. **10**, 509 (1968).

[24] D. R. Smith and N. Kroll, Phys. Rev. Lett. **85**, 2933 (2000).

[25] R. A. Shelby, D. R. Smith, and S. Schultz, Science **292**, 77 (2001).

[26] C. G. Parazzoli, R. B. Greegor, K. Li, B. E. C. Koltenbah, and M. Tanielian, Phys. Rev. Lett. **90**, 107401 (2003).

[27] C. Enkrich, M. Wegener, S. Linden, S. Burger, L. Zschiedrich, F. Schmidt, J. F. Zhou, T. Koschny, and C. M. Soukoulis, Phys. Rev. Lett. **95**, 203901 (2005).

[28] J. Zhou, T. Koschny, , M. Kafesaki, E. N. Economou, J. B. Pendry, and C. M. Soukoulis, Phys. Rev. Lett. **95**, 223902 (2005).

[29] W. J. Padilla, A. J. Taylor, C. Highstrete, M. Lee, and R. D. Averitt, Phys. Rev. Lett. **96**, 107401 (2006).

[30] L. D. Landau, E. M. Lifshitz, and L. P. Pitaevskii, *Electrodynamics of Continuous Media* (Butterworth-Heinemann, Oxford, 1984).

[31] M. Notomi, Phys. Rev. B **62**, 10696 (2000).

[32] C. Luo, S. G. Johnson, J. D. Joannopoulos, and J. B. Pendry, Phys. Rev. B **65**, 201104 (2002).

[33] A. Berrier, M. Mulot, M. Swillo, M. Qiu, L. Thyln, A. Talneau, and S. Anand, Phys. Rev. Lett. **92**, 073902 (2004).

[34] P. V. Parimi, W. T. T. Lu, P. Vodo, and S. Sridhar, Nature **426**, 404 (2003).

[35] E. Cubukcu, K. Aydin, E. Ozbay, S. Foteinopoulou, and C. M. Soukoulis, Nature **423**, 604 (2003).

[36] V. M. Agranovich, Y. R. Shen, R. H. Baughman, and A. A. Zakhidov, Phys. Rev. B **69**, 165112 (2004).

[37] C. Luo, S. G. Johnson, J. D. Joannopoulos, and J. B. Pendry, Phys. Rev. B **68**, 45115 (2003).

[38] D. R. Smith, D. Schurig, M. Rosenbluth, S. Schultz, S. A. Ramakrishna, and J. B. Pendry, App. Phys. Lett. **82**, 1506 (2003).

[39] Z. Lu, J. A. Murakowski, C. A. Schuetz, S. Shi, G. J. Schneider, and D. W. Prather, Phys. Rev. Lett. **95**, 153901 (2005).

[40] N. Fang, H. Lee, C. Sun, and X. Zhang, Science **308**, 534 (2005).

[41] D. O. S. Melville and R. J. Blaikie, Optics Express **13**, 2127 (2005).

[42] J. M. Vigoureux and D. Courjon, Appl. Opt. **31**, 3170 (1992).

[43] X. Wang, Optics Express **12**, 2919 (2004).

[44] X. Hu and C. T. Chan, App. Phys. Lett. **85**, 1520 (2004).

[45] X. Zhang, Phys. Rev. B **70**, 195110 (2004).

[46] E. Cubukcu, K. Aydin, E. Ozbay, S. Foteinopoulou, and C. M. Soukoulis, Phys. Rev. Lett. **91**, 207401 (2003).

[47] Z. Y. Li and L. L. Lin, Phys. Rev. B **68**, 245110 (2003).

[48] X. Zhang, Phys. Rev. B **70**, 205102 (2004).

[49] S. L. He, Z. C. Ruan, L. Chen, and J. Shen, Phys. Rev. B **70**, 115113 (2004).

[50] P. Belov, C. Simovski, and P. Ikonen, Phys. Rev. B **71**, 193105 (2005).

[51] X. Zhang, Z. Q. Zhang, and C. T. Chan, Phys. Rev. B **63**, 081105 (2001).

[52] C. Jin, B. Cheng, B. Man, Z. Li, D. Z. Zhang, S. Ban, and B. Sun, App. Phys. Lett. **75**, 1848 (1999).

[53] A. E. Carlsson, Phys. Rev. B **47**, 2515 (1993).

[54] S. David, A. Chelnikov, and J. M. Lurtioz, IEEE Quantum Electron. **37**, 1427 (2001).

[55] M. A. Kaliteevski, S. Brand, A. Abram, T. F. Krauss, P. Millar, and R. M. de la Rue, J. Phys. Condens. Matter **13**, 10459 (2001).

[56] X. Zhang, Z. Li, B. Cheng, and D. Z. Zhang, Optics Express **15**, 1292 (2007).

[57] C. Kittel, *Introduction to Solid State Physics* (Wiley, Berkeley, 2004).

[58] J. D. Jackson, *Classical Electrodynamics* (Wiley, New York, 1998).

[59] K. M. Leung and Y. F. Liu, Phys. Rev. Lett. **65**, 1646 (1990).

[60] H. S. Sözüer, J. W. Haus, and R. Inguva, Phys. Rev. B **45**, 13962 (1992).

[61] H. S. Sözüer and J. W. Haus, J. Opt. Soc. Am. B **10**, 296 (1993).

[62] K. M. Ho, C. T. Chan, and C. M. Soukoulis, Phys. Rev. Lett. **65**, 3152 (1990).

[63] P. R. Villeneuve and M. Piché, J. Mod. Opt. **41**, 241 (1994).

[64] S. G. Johnson and J. D. Joannopoulos, Optics Express **8**, 173 (2001).

[65] K. Sakoda, *Optical Properties of Photonic Crystals* (Springer, Berlin, 2005).

[66] S. G. Johnson and J. D. Joannopoulos, The MIT Photonic-Bands Package home page, `http://ab-initio.mit.edu/mpb/`.

[67] R. D. Meade, A. M. Rappe, K. D. Brommer, J. D. Joannopoulos, and O. L. Alerhand, Phys. Rev. B **48**, 8434 (1993).

[68] S. G. Johnson, Phys. Rev. B **55**, 15942 (1997).

[69] T. Suzuki and P. K. L. Yu, Phys. Rev. B **57**, 2229 (1998).

[70] K. Busch and S. John, Phys. Rev. Lett. **83**, 967 (1999).

[71] M. Frigo and S. G. Johnson, in *FFTW: an adaptive software architecture for the FFT*, Institute of Electrical and Electronics Engineers (Proc. 1998 IEEE Intl. Conf. on Acoustics, Speech, and Signal Processing, New York, 1998), p. 1381.

[72] L. C. Andreani and M. Agio, IEEE J. Quantum Electronics **38**, 891 (2002).

[73] M. Plihal and A. A. Maradudin, Phys. Rev. B **44**, 8565 (1991).

[74] S. Ismaili-Beigi and T. A. Arias, Comp. Phys. Commun. **128**, 1 (2000).

[75] A. Taflove and S. C. Hagness, *Computational Electrodynamics: The Finite-Difference Time-Domain Method* (Artech, Norwood, MA, 2000).

[76] K. Yee, Antennas and Propagation, IEEE Transactions **14**, 302 (1966).

[77] S. G. Johnson and J. D. Joannopoulos, The MIT Electromagnetic Equation Propagation home page, `http://ab-initio.mit.edu/index.php/meep/`.

[78] J. P. Berenger, Journal of Computational Physics **114**, 185 (1994).

[79] M. Oxborrow and C. L. Henley, Phys. Rev. B **48**, 6966 (1993).

[80] E. Di Gennaro and A. Andreone, private communication, 2008.

[81] Y. G. Roh, T. Tanabe, A. Shinya, H. Taniyama, E. K. S. Matsuo, T. Saro, and M. Notomi, Phys. Rev. B **81**, 121101 (2010).